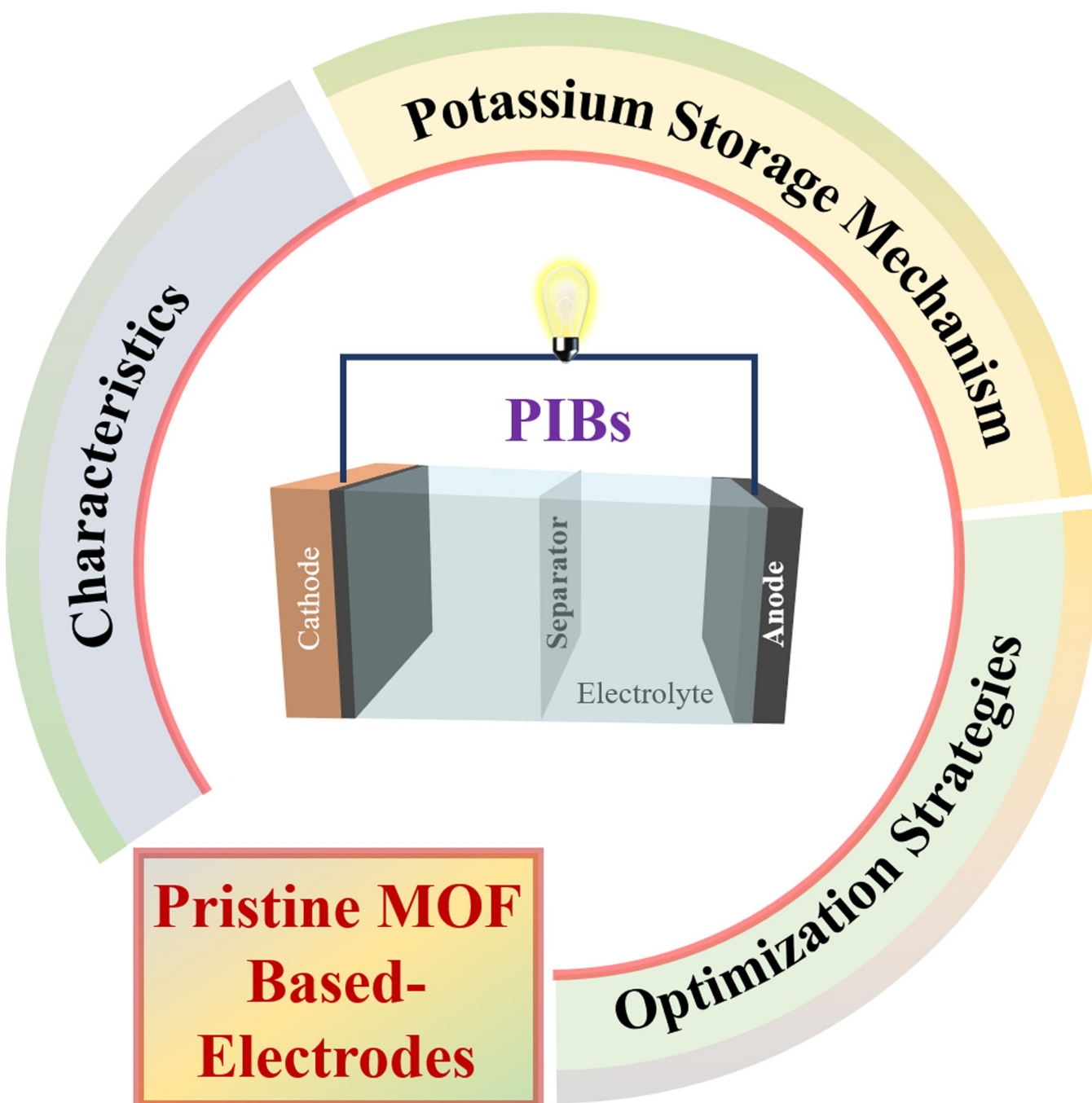


Recent Advances on Pristine MOF-Based Electrodes for PIBs: Characteristics, Potassium Storage Mechanisms, and Optimization Strategies

Chao Li,*^[a] Hong Yan,^[a] Hanlu Yang,^[a] Min Yue,^[a] Shujun Li,^[a] and Kuaibing Wang*^[b]



Benefiting from the natural attributes of exceptional chemical stability, versatility, porous structure, and tunable pore sizes, pristine metal-organic frameworks, MOFs, have gained widespread recognition as advanced anodes and cathodes for potassium-ion batteries, PIBs, showcasing several promising features in electrochemical energy storage devices. Here, a comprehensive review highlights recent advancements in

pristine MOF-based electrodes for PIBs, focusing on the detailed characteristics, redox reaction monachism, and effective strategies to improve electrochemical energy performance, which provides guidance for further developments in electrode design and optimization strategies aimed at achieving prolonged cyclability and capacity retention.

1. Introduction

Recently, there has been increasing interest in potassium-ion batteries (PIBs) as potential substitutes for lithium-ion batteries (LIBs) in the field of materials science and electrochemical energy storage system.^[1–3] PIBs, a type of rechargeable battery utilizing potassium ions (K-ions, K⁺) as charge carriers instead of lithium ions (Li-ions, Li⁺), exhibit a working mechanism akin to LIBs, boasting advantages such as low cost, high energy density, and eco-friendliness.^[4–6] Moreover, they offer benefits such as greater abundance and lower cost compared to lithium, an intermediate K⁺/K standard reduction potential (-2.93 vs. SHE) lying between that of Li⁺/Li (-3.04 V vs. SHE) and Na⁺/Na (-2.71 V vs. SHE),^[7–10] and enhanced K-ions transport kinetics facilitated by the highest ionic conductivity among Na-ions and Li-ions in organic electrolytes, attributed to the larger Stokes radius of K-ions (see Figure 1). These attributes position PIBs as a viable option for application in large-scale energy storage.^[11–13] Nonetheless, despite PIBs exhibiting promising features, the widespread adoption of these energy storage systems faces several challenges, including electrode volume fluctuations during charging and discharging processes due to the ultra-high ionic radius of K⁺ and limited rate performance resulting from low K⁺ diffusion rates within specific crystal structural electrodes.^[14–18] Therefore, the exploration of novel electrode materials is imperative to sustain the exceptional performance characteristics of PIBs.

Metal-organic frameworks (MOFs), characterized by metal cation nodes and organic building linkers,^[19–27] have seen widespread use since their inception in the late 1990s and early 2000s,^[28–37] attributed to the pioneering work of Omar M. Yaghi and his research team's development of MOF-5 in 1999.^[38] MOF-5, comprising zinc oxide clusters linked by benzene dicarboxylate ligands, represented a groundbreaking achievement, demonstrating the feasibility of designing crystalline materials with high surface areas and customizable pore sizes. This milestone sparked extensive research into MOF synthesis and applications,^[39–48] yielding a variety of materials with diverse

properties.^[49–58] Beyond the pivotal MOF-5, researchers have pursued novel synthetic approaches and investigated a range of metal ions and organic ligands,^[59–62] leading to the development of MOFs with varying surface areas, pore sizes, and chemical functionalities,^[63–85] making them ideal candidates for advanced electrodes in high-performance PIBs.^[86–88] Recent attention from researchers has shifted towards designing pristine MOF electrodes and MOF derivatives-based electrodes and examining the redox reaction mechanisms of MOF derivatives. Effective strategies to enhance the overall electrochemical properties of PIBs have also been a focus.^[89–91] Nevertheless, the predominant focus in previous reviews of electrodes related to MOFs for PIBs has been on accentuating the mechanisms of redox reactions and the electrochemical performances of MOF derivatives, including but not limited to metal oxides, sulfides, and selenides. Meanwhile, the energy storage mechanism of MOF derivatives primarily relies on alloying reactions rather than intercalation reactions. This results in high capacity but poor long-cycle performance due to significant volume expansion. Conversely, pristine MOFs mainly undergo intercalation reactions, rarely alloying reactions, offering satisfactory electrochemical properties thanks to their robust framework and porous nature.^[92–94]

This concentration has resulted in an oversight of the exploration concerning original MOF electrodes. In these particular cases, the transformation of MOFs into derivatives, achieved through processes such as calcination or other treatments related to batteries, leads to the forfeiture of organic ligands. This alteration markedly diminishes the quantity of active sites present in the initial pristine MOF structures, presenting challenges such as the generation of precursor waste, heightened industrial costs, and impracticality for broad-scale application.^[95,96] Conversely, the inherent organic ligands within pristine MOFs can undergo complete activation, actively contributing to energy storage devices.^[97–99] A thorough comprehension of the storage mechanisms pertaining to both organic ligands and metal cations within pristine MOFs imparts valuable insights for propelling the development of high-performance MOF-based electrodes within electrochemical energy batteries. As a result, this review extensively underscores recent progressions in pristine MOF-based electrodes for PIBs (see detail in Scheme 1), with a specific focus on intricate characteristics, redox reaction monachism, and efficacious strategies to enhance electrochemical energy performance, furnishing guidance for subsequent advancements in electrode design and optimization strategies, with the ultimate aim of achieving prolonged cyclability and capacity retention.

[a] Dr. C. Li, H. Yan, H. Yang, Dr. M. Yue, Dr. S. Li
School of Physics and Electronic Engineering
Sichuan University of Science & Engineering
Yibin 644000, P. R. China
E-mail: chaolicc@outlook.com

[b] Prof. K. Wang
Department of Chemistry and College of Sciences
Nanjing Agricultural University
Nanjing 210095, P. R. China
E-mail: wangkb@njau.edu.cn

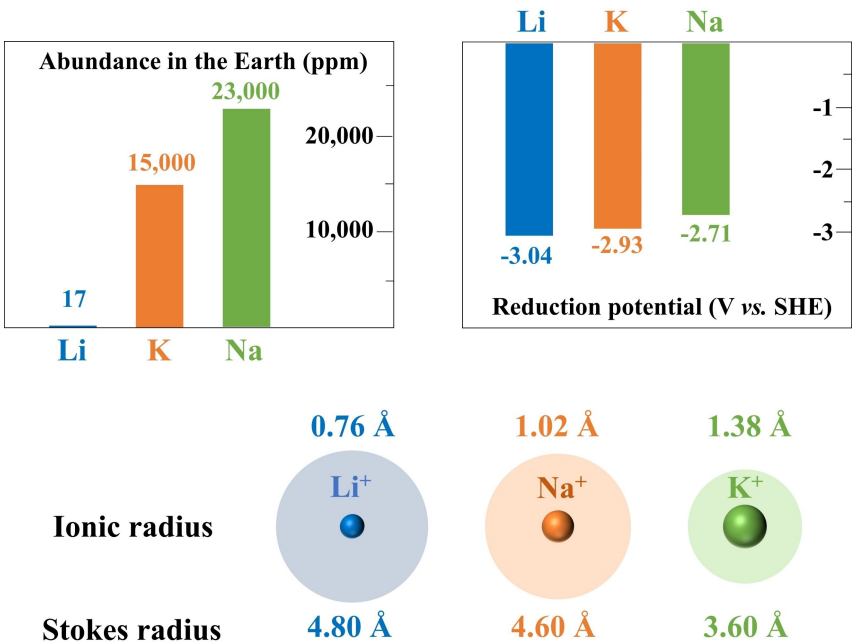


Figure 1. Comparison of the Li, Na, and K metal elements abundance in the Earth, reduction potentials as well as Ionic/Stokes radius.

2. Pristine MOF Anodes for PIBs

As mentioned before, MOFs are porous materials constructed from redox-active metal cations and organic ligands, exhibiting customizable pore sizes and elevated surface areas. The pristine MOFs refer to MOFs in their initial and unaltered state, which retain the quantity of active sites within the original MOF structures in an unmodified condition. Anticipating the K^+ storage performance akin to that of Li^+ in LIBs, various pristine MOFs were utilized as anodes to explore their K^+ storage capability in PIBs due to their distinctive characteristics, such as high porosity, potential for reversible K^+ storage, and a secure redox potential preventing the formation of K metal during battery operation.

2.1. Characteristics of Pristine MOF Anodes for PIBs

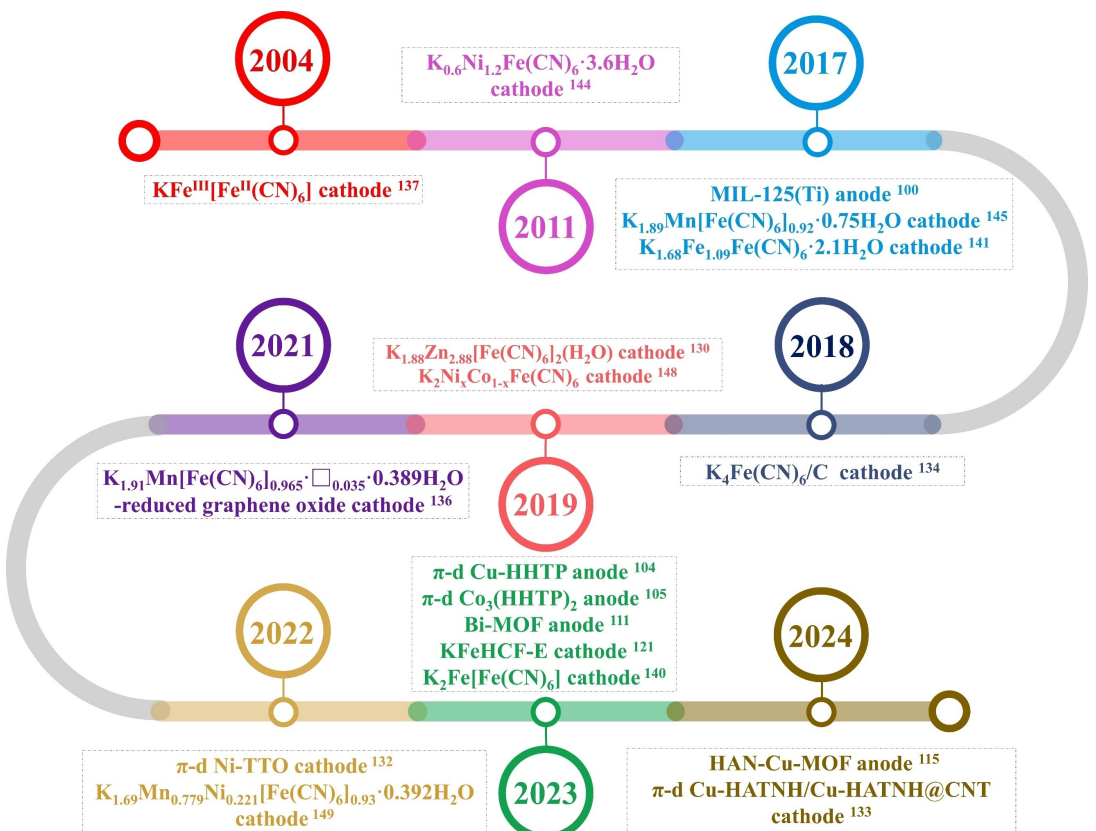
In the utilization as anodes for PIBs, the pristine MOFs typically exhibit a configuration consisting of metal nodes connected by organic ligands to form a three-dimensional (3D) porous framework, such as Materials of Institute Lavoisier (MIL)^[100–102] and various carboxylate MOFs,^[103] where the metal nodes could encompass diverse transition metals, such as zinc, copper, or iron, and the organic ligands commonly consist of carboxylate groups ($\text{COO}-\text{R}$). Such as MIL-125(Ti) MOF,^[100] MOF-235,^[101] MIL-47,^[102] among others. Simultaneously, the new emerging π -d conjugated MOFs, constructed using transition-metal nodes and planar π -conjugated organic ligands with two-dimensional (2D) frameworks and high conductive based on their inherent π -conjugated structures, have also been delivered as advanced anodes for PIBs. For instance, π -conjugated Cu-MOF anodes,^[104] π -conjugated Co-MOF anodes,^[105] and π -conjugated Ni-MOF anodes.^[106] Regardless of whether they are 3D or 2D pristine



Chao Li is currently a lecturer at the School of Physics and Electronic Engineering, Sichuan University of Science & Engineering. He received his Ph.D. degree at the School of Materials and Energy, Materials Science and Engineering, University of Electronic Science and Technology of China. From 2019 to 2020, he joined Prof. Qichun Zhang's group as a joint PhD student at the School of Materials Science and Engineering, Nanyang Technological University, Singapore. His research interests involve organic energy storage materials and their applications, particularly, novel electrode materials as well as new designs for energy storage devices.



Kuaibing Wang is an associate professor of the Department of Chemistry and College of Sciences, Nanjing Agricultural University, P.R. China. In 2013, he received his Ph.D. under the supervision of Prof. Zhilin Wang in the Department of Chemistry and Chemical Engineering from Nanjing University. He worked at Prof. Qichun Zhang's group in 2019 as a visiting scholar at the School of Materials Science and Engineering, Nanyang Technological University, Singapore. His research interests focus on the controllable fabrication and application of 2D MOFs, bulky/nano-MOFs, and MOF-derived inorganic hybrid materials for the energy-storage application.



Scheme 1. Timeline of significant milestones in the development of pristine MOF electrodes for Potassium-ion batteries.

MOF anodes, the choice of metal and ligand could be customized to attain specific properties, thereby enhancing the electrochemical properties of the anode material. Consequently, the selection of metal and ligand influences the structure, stability, and electrochemical properties of pristine MOF-based anodes for PIBs. For example, the MIL-125(Ti),^[100] MOF-235,^[101] and MIL-47 anodes,^[102] all employing terephthalic acid ligands but with different metal ions, demonstrate distinct electrochemical performance. Similarly, Co-MOF^[103] and π-conjugated Co₃(HHTP)₂^[105] anodes, sharing the same Co-metal center but featuring different organic ligands, exhibit unique electrochemical properties.

In light of these findings, the design of pristine MOF-based anodes for PIBs should be meticulous, featuring a distinctive architecture with specific metal ions and organic ligands. This architectural uniqueness is crucial, as it establishes an interconnected metal-ligand network that forms a porous structure with well-defined channels and void spaces. This arrangement provides an expansive surface area conducive to electrochemical redox reactions, facilitates swift K⁺ diffusion, and enables efficient storage of charge carriers.

2.2. Potassium Storage Mechanism of Pristine MOF Anodes for PIBs

Operating within the identical voltage range as anodes for PIBs, distinct pristine MOFs with varying chemical structures have demonstrated a shared potassium storage mechanism, specifically intercalation reactions. This mechanism, governed by the redox couples, is crucial owing to the inherent open framework architecture of these MOFs, delivering satisfied specific capacities, rate performance, and long-cycle properties.^[107] However, they exhibit dissimilar redox-active entities, such as V⁴⁺/V³⁺,^[102] V³⁺/V²⁺,^[102] Co³⁺/Co²⁺,^[108] Co²⁺/Co⁰,^[103] C=O/C-O^[101] redox active pairs, and so forth, relying on the in-situ or ex-situ measurements and density functional theory calculations, e.g., UiO-66^[109,110] could obtain a high theoretical capacity of 644 mAh g⁻¹ and highlighting that appropriate modifications to UiO-66 could enhance its porosity, electronic conductivity, as well as ionic conductivity when employed as anode material for PIBs. Furthermore, alloying reaction along with intercalation reaction mechanisms could be relevant to a select few unique MOFs, demonstrating superior specific capacities but suffering from inadequate rate performance and extended cycling durability due to significant volume expansion, like Bi-MOFs,^[111] in which the alloying reactions between Bi and K-ions coupled with K-ions insertion/reaction within carboxylate groups depict the energy storage mechanism of Bi-MOFs as potential anodes for PIBs.

In summary, to effectively guide the design and enhancement of PIBs performance, the investigation of the distinct redox reaction couples for potassium storage mechanisms in various MOF-based electrodes is a fundamental requirement for their practical implementation within PIB systems.

2.3. Optimization Strategies of Pristine MOF Anodes for PIBs

Optimizing pristine MOF-based anodes for PIBs involves various strategies to enhance their electrochemical performance, such as nano-structural 3D MOFs, Conductive π -d conjugated MOFs, and MOF-carbon composites. The primary objective is to improve critical factors such as capacity, coulombic efficiency, cycling stability, rate capability, and overall efficiency.

2.3.1. Nano-Structural 3D MOFs

Various pristine 3D MOF anodes for PIBs are almost reliant on the same carboxylate acid ligands, i.e., terephthalic acid (H_2BDC), with distinct metal centers and unique metal-salt combinations. Meanwhile, the micro-porous structural and the nano-structural 3D MOFs contribute to high surface areas and expansive pore volumes, along with the multitude of pore

dimensions and topologies that could benefit facile K-ions insertion/removal during the cycling process, resulting in superior electrochemical performance. As demonstrated in Figure 2a, Feng et al. synthesized MIL-125(Ti)^[100] with H_2BDC ligand, showcasing a micro-porous configuration characterized by an average pore size of approximately 1.60 nm, resulting in a 58.86% initial coulombic efficiency and a significant capacity of 208 mAh g⁻¹ within 10 mA g⁻¹, guessing the redox mechanism relay on the organic component, which includes the benzene ring and carboxylate groups, as well as the metal ions. Meanwhile, based on the same H_2BDC ligand, Deng et al. proposed a micro-porous MOF-235 Fe-based MOF,^[101] displaying a hexagonal bipyramidal shape with particle sizes ranging between 200 nm and 2,000 nm, gained an initial coulombic efficiency of 45.3%, but showcased a relatively low capacity due to the not participate Fe^{3+} and solely the redox active C=O/C—O couple. Conversely, differs from the MOF-235, L-Co₂(OH)₂BDC,^[103] a Co-MOF based on the same H_2BDC ligand with layered crystalline architecture with micron-sized crystals, gaining a relatively high initial coulombic efficiency of 60.65% and a large capacity of 246 mAh g⁻¹ within 100 mA g⁻¹ attributed to the redox active Co centers and organic ligands, as investigated by Co K-edge X-ray absorption near-edge structure and O K-edge soft X-ray spectroscopy measurements (Figure 2b). Moreover, the bifunctional vanadium-based MOF, MIL-47,^[102] relying on H_2BDC ligand, served as both an anode and cathode for PIBs designed

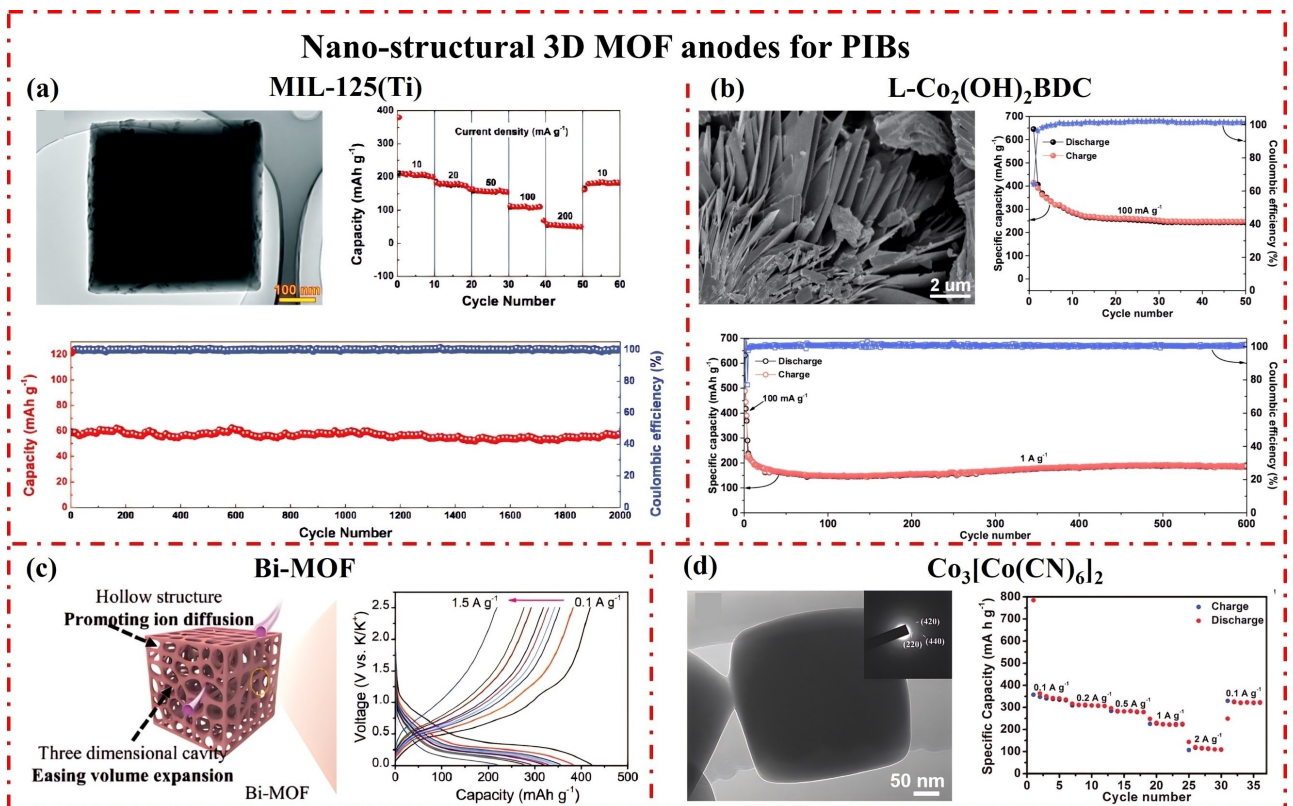


Figure 2. The structure characteristics and electrochemical performance of Pristine nano-structural 3D MOF Anodes for optimization PIBs. a) MIL-125(Ti). Reproduced with permission from Ref. [100]. Copyright (2017) Royal Society of Chemistry; b) L-Co₂(OH)₂BDC. Reproduced with permission from Ref. [103]. Copyright (2017) Elsevier; c) Bi-MOF. Reproduced with permission from Ref. [111]. Copyright (2022) Wiley-VCH.; d) PBA, Co₃[Co(CN)₆]₂. Reproduced with permission from Ref. [108]. Copyright (2018) Wiley-VCH..

by Deng and co-workers. When delivered as an anode, MIL-47 obtained a capacity of 272 mAh g⁻¹ within 10 mA g⁻¹ contributing to the reversible enolization process of conjugated carbonyl of terephthalic acid alongside the partly valence change of vanadium ions. Meanwhile, recently, a Bi-MOF^[111] was synthesized using H₂BDC and Bi(NO)₃ as precursor materials to serve as anodes for PIBs. As illustrated in Figure 2c, Bi-MOF exhibited a network framework featuring numerous hollows that facilitate electrolyte infiltration and promote rapid ion diffusion three reversible pairs of redox peaks were observed in Bi-MOF, indicating the alloying reactions between Bi and K⁺ as well as insertion/extraction reactions between H₂BDC and K⁺ in a mixed reaction process. The initial Coulombic efficiency of Bi-MOF was relatively low with 38%. Despite this, Bi-MOF exhibited commendable electrochemical performance, showcasing a high reversible capacity of 415 mAh g⁻¹ after 500 cycles within 100 mA g⁻¹. Furthermore, the cycling stability was excellent, maintaining a capacity of 315 mAh g⁻¹ at 500 mA g⁻¹ over an extended period. Furthermore, PBAs have recently been delivered as anodes for PIBs, demonstrating satisfactory electrochemical performance. For example, as displayed in Figure 2d, the PBA, Co₃[Co(CN)₆]₂,^[108] designed by Zhu and co-workers, obtaining a well-defined cube shape with dimensions ranging from 200 to 300 nm and showcasing a 46% initial coulombic efficiency and a substantial capacity of 324.5 mAh g⁻¹ within 100 mA g⁻¹ relying on both electrochemically active carbon- and nitrogen-coordinated cobalt, resulting in the generation of Co metal nanoparticles and Co (I) during the potassiation process. Subsequently, Esdras J. Canto-Aguilar et al. conducted an in-depth exploration of the detailed electrochemical performance of a series of PBAs, M₃[Co(CN)₆]₂ (M=Cu, Co, Ni, Zn),^[112] unveiling that a heightened interaction of dipole-dipole between interstitial water and the framework has led to the spontaneous occurrence of redox processes at the boundary of the electrolyte and the electrode during open-circuit circumstances. This phenomenon restricts the suitability of PBAs in PIB anodes. Additionally, the capacity retention of PBA MOF electrodes was found to be contingent not only solely on the external metal but also on the discharge cut-off potential.

2.3.2. Conductive π-d Conjugated MOFs

Conductive π-conjugated MOFs present several advantages when utilized as anodes in PIBs. Firstly, their high surface area and porous structure facilitate improved K⁺ diffusion and storage, resulting in enhanced electrochemical performance. Additionally, the incorporation of π-conjugated systems within the MOF structure boosts electrical conductivity, ensuring efficient charge and discharge processes. This conductivity is crucial for maintaining stable cycling performance and achieving high specific capacity over multiple charge-discharge cycles. Furthermore, the tunable nature of MOFs allows for the optimization of their chemical and structural properties, enabling the design of anodes with tailored characteristics for specific battery applications. Overall, the integration of conductive π-conjugated MOFs as anodes in PIBs holds promise for

creating high-performance energy storage systems with enhanced durability and efficiency. Recently, various conductive π-d conjugated MOFs have been delivered as novel anodes for PIBs, obtaining improved electrochemical performance beneficial to the enhanced conductive, which is regarded as one of the most optimization strategies of pristine MOF anodes for PIBs.

For example, as illustrated in Figure 3a, P1-NiBTA,^[106] a Ni-based MOF derived from 1,2,4,5-tetraaminobenzene (BTA) and Ni-salt, achieved a high capacity of 220 mAh g⁻¹ within 100 mA g⁻¹, demonstrating excellent rate properties (104 mAh g⁻¹ within 10,000 mA g⁻¹), with two-electrons potassiation-depotassiation, where Ni²⁺ did not participate in redox reactions. Subsequently, to deeply explore the K-ions storage mechanisms of NiBTA, Kapaev et al.^[113] employed advanced theoretical and experimental methodologies, encompassing in-situ/ex-situ XRD/XANES and in-situ Raman spectroscopy. As displayed in Figure 3b, NiBTA gained a capacity of 280 mAh g⁻¹ within 100 mA g⁻¹ with an average depotassiation potentials of 1.35 V vs. K⁺/K, while, indicating that the potassium storage mechanism of NiBTA involves two-electron reversible redox reaction for each repeating units along with the absorption bandgap changes at the molecular level. Even with the potentials as low as 0 V vs. K⁺/K, there was no more than two electron reduction reactions per repeating unit in NiBTA. Meanwhile, based on the same nitrogen ligation site, Troshin et al. synthesized a one-dimensional π-d conjugated Ni-MOF, Ni-DAB,^[114] using a distinct ligand of 3,3'-diaminobenzidine (DAB). In contrast to TAB, DAB is a cost-effective and stable compound, which was extensively employed in immunochemical staining. As a result, as shown in Figure 3c, Ni-DAB obtained a capacity of 158 mAh g⁻¹ within 1,000 mA g⁻¹, experiencing a mere 8.6% capacity fade after 600 cycles. This performance demonstrated a similar K-ions storage mechanism to NiBTA, indicating the same aromatization of the DAB ligands upon potassiation through a two-electron redox reaction.

Beyond nitrogen, oxygen could also serve as a ligation site for constructing π-d conjugated MOFs. E.g., Liu et al. employed the ligand hexahydroxytriphenylene (HHTP) to synthesize a novel conductive π-d conjugated Co-MOF, Co₃(HHTP)₂,^[105] via liquid-phase method. As displayed in Figure 3d, Co₃(HHTP)₂ showcased a cross-linked porous network morphology with the nanowires and exhibited a substantial reversible specific capacity (332 mA h g⁻¹ at 100 mA g⁻¹), exceptional long-cycle stability maintaining a capacity of 230 mA h g⁻¹ within 1,000 mA g⁻¹ after 700 cycles), and an excellent rate performance delivering a capacity of 165 mAh g⁻¹ within 4,000 mA g⁻¹, attributed to the promoted potassium-ion diffusion and electron transfer facilitated by a multitude of active sites and open pathways, unveiling an 8-electron transfer potassium storage mechanism as revealed by various ex-situ XPS spectra, FTIR spectra, and Raman spectra. Subsequently, Han et al. developed a Cu-HHTP^[104] conductive π-d conjugated MOFs using the same ligand of HHTP but gained a relatively poor electrochemical property with a capacity of 109 mAh g⁻¹ within 100 mA g⁻¹ due to the sole potassium ion storage in benzene ring. Recently, a π-d conjugated HAN-Cu-MOF,^[115] synthesized through a sol-

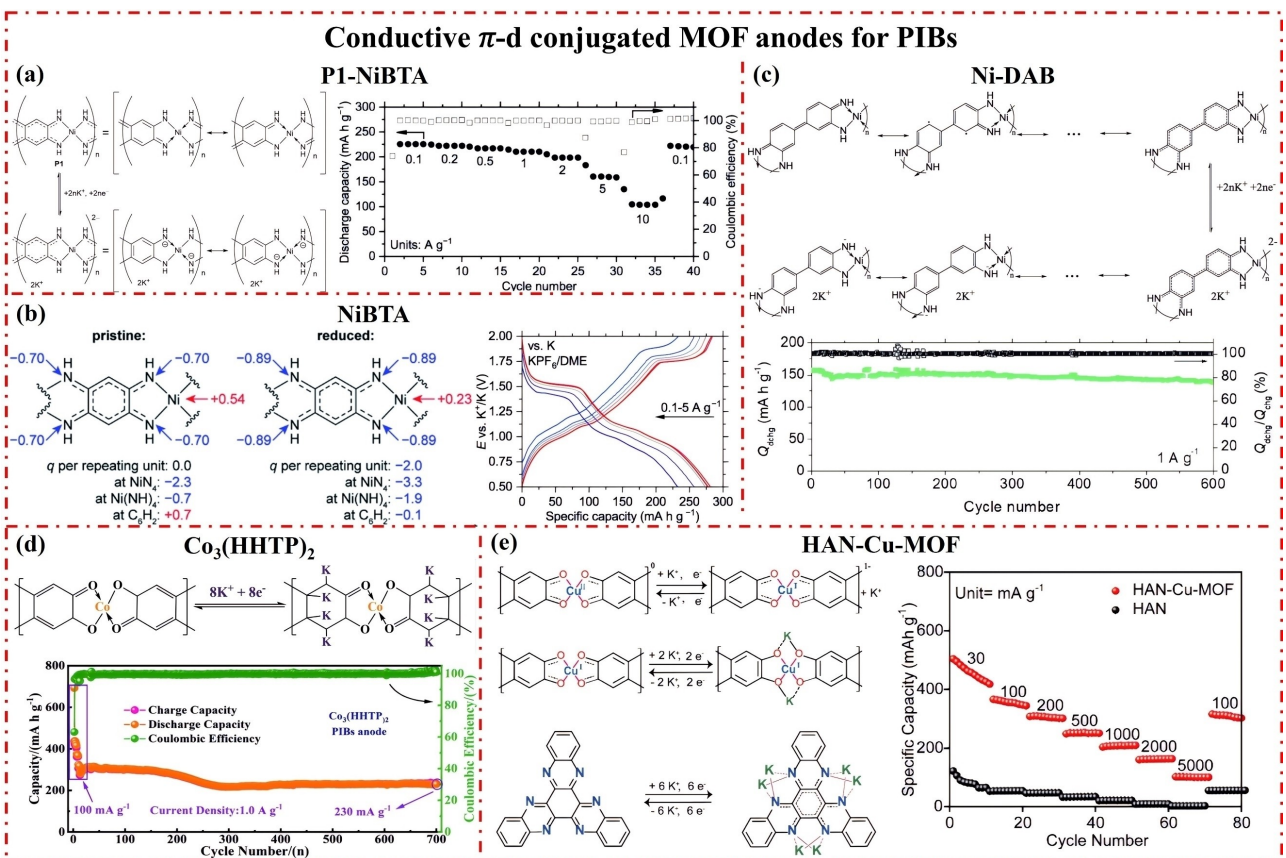


Figure 3. The structure characteristics and electrochemical performance of pristine conductive π -d conjugated 3D MOF anodes for optimization PIBs. a) P1-NiBTA. Reproduced with permission from Ref. [106]. Copyright (2020) Royal Society of Chemistry; b) NiBTA. Reproduced with permission from Ref. [113]. Copyright (2022) Royal Society of Chemistry. c) Ni-DAB. Reproduced with permission from Ref. [114]. Copyright (2020) Wiley-VCH; d) Co₃(HHTP)₂. Reproduced with permission from Ref. [105]. Copyright (2022) Royal Society of Chemistry. e) HAN–Cu-MOF. Reproduced with permission from Ref. [115]. Copyright (2024) American Chemical Society.

ution reaction involving Cu(NO₃)₂ and HAN-6OH, was explored as anodes for both high-temperature and room-temperature PIBs. As illustrated in Figure 3e, HAN–Cu-MOF, constructed by utilizing N-rich HAN molecules and CuO₄ units through π -d conjugation, provides a wealth of accessible redox-active sites, facilitating high-capacity potassium-ion storage based on a surface-dominated storage mechanism. Meanwhile, the porous reticular architecture with a π -d conjugated structure in HAN–Cu-MOF not only imparts robustness to resist solubility in organic electrolytes but also sustains the repetitive intercalation and deintercalation of K-ions. Additionally, this structure establishes an efficient channel for rapid K⁺/e⁻ transfer. As a result, these distinctive attributes position the MOF as a high-performance anode for PIBs, even under 60 °C. Remarkably, HAN–Cu-MOF demonstrated impressive electrochemical properties with a superior specific capacity of 455 mAh g⁻¹ at 50 mA g⁻¹.

2.3.3. MOF-Carbon Composites

MOF-carbon composites present notable advantages when utilized as anodes for PIBs. The combination of carbon materials

with MOFs results in a synergistic blend of properties, encompassing high surface area, exceptional conductivity, and robust structural stability. This distinctive amalgamation enhances the overall electrochemical performance of the anode, enabling efficient potassium-ion storage and facilitating rapid charge/discharge cycles. Additionally, MOFs contribute to increased potassium-ion diffusion kinetics and provide numerous active sites for electrochemical reactions. The carbon matrix further ensures mechanical integrity and alleviates volume expansion during cycling, leading to extended cycle life and superior overall battery performance.

Whether considering 3D carbonylated acid base-MOFs or Conductive π -d conjugated MOFs, the integration of MOFs and carbon materials offers a promising avenue for advancing PIBs technology, addressing key challenges, and laying the foundation for more sustainable and high-performing energy storage solutions. For instance, through the in-situ compositing with high aspect ratio multiwall-carbon tubes (MCNTs), Deng et al. prepared various MOF-235/MCNTs composites,^[101] where the MCNTs effectively attached to the MOF-235 crystal surface. As a result, among these composites, MOF-235 + 20 M exhibited a relatively high electronic conductivity of 3×10^{-4} S cm⁻¹ compared to pristine MOF-235 (2×10^{-7} S cm⁻¹) and gained a

capacity of 187 mAh g^{-1} within 20 mA g^{-1} along with the 29.1% initial coulombic efficiency (Figure 4a) attributed to redox-active carboxyl group of $\text{TP}^{2-}/\text{TP}^{4+}$. Additionally, Deng et al. demonstrated the incorporation of high specific surface area graphene (G) with MOF-235 to enhance the poor electronic conductivity of pristine MOF-235.^[101] with the combining of G with MOF-235, MOF-235+20G exhibited an improved conductivity ($2 \times 10^{-3} \text{ S cm}^{-1}$ vs. $2 \times 10^{-7} \text{ S cm}^{-1}$ for pristine MOF-235), enhanced electrochemical performance (180 mAh g^{-1} within 200 mA g^{-1}), along with an increased initial coulombic efficiency of 31.2%.

Furthermore, MOF-carbon composites could enhance the electrochemical performance of conductive π -d conjugated MOFs. For example, Han et al. designed MOF-carbon composites, Cu-HHTP/G,^[104] through the in-situ synthesis of the conductive π -d conjugated Cu-HHTP on graphene (G) layers. As demonstrated in Figure 4b, Cu-HHTP nanorods formed a two-dimensional (2D) continuous conductive network by uniformly distributed and enveloped within layered graphene. As a result, Cu-HHTP/G exhibited a higher initial coulombic efficiency of 47.68% than that of the pristine Cu-HHTP (42.62%), obtained a higher reversible capacity of 226 mAh g^{-1} within 100 mA g^{-1} than that of pristine Cu-HHTP (109 mAh g^{-1}), despite relying solely on the redox-active benzene ring and not involving Cu ions for potassium ion storage.

In summary, Pristine MOFs exhibit great potential as anodes for potassium-ion batteries, presenting numerous benefits in energy storage applications. Their inherent characteristics, including a high surface area and porosity, facilitate the effective diffusion of potassium ions, thereby enhancing electrochemical performance. The electrochemical characteristics of the pristine MOF anode reported for PIBs are illustrated

in Table 1. Crafting pristine MOF anodes involves a meticulous approach to designing and synthesizing MOF structures with tailored characteristics to optimize their electrochemical properties. The adjustability of MOFs enables the customization of their chemical and structural features, further boosting their effectiveness as anodes. Looking forward, ongoing research and development in pristine MOF anodes are anticipated to yield more advanced materials, offering solutions to challenges in potassium-ion batteries, such as enhancing specific capacity, cycling stability, and overall energy density. The outlook suggests that pristine MOFs hold substantial promise in advancing potassium-ion battery technology, contributing to the creation of efficient and sustainable energy storage solutions.

3. Pristine MOF Cathodes for PIBs

As mentioned previously, pristine MOFs have been delivered as anodes for PIBs. Meanwhile, recently, benefiting from the highly tunable structures allowing for the customization of electrochemical properties through synthetic manipulation, the distinctive pore configurations and surface functional groups of MOFs creating effective ion transport pathways and sites for K-ions insertion/extraction, and the extensive specific surface areas providing numerous active sites conducive to K-ions storage and release, pristine MOFs have also garnered attention not only as potential anodes but also as cathodes for PIBs. These factors contribute to an augmentation in the electrode energy storage capacity, an enhancement in cycling stability, and an increase in energy density, thereby elevating the overall

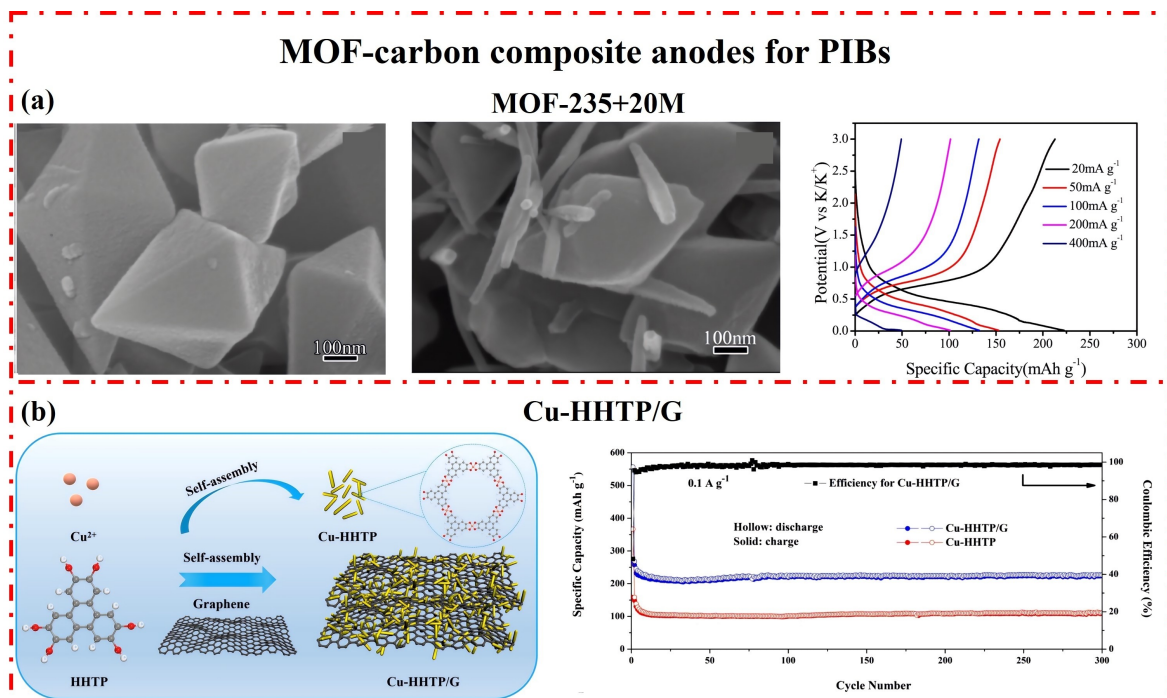


Figure 4. The structure characteristics and electrochemical performance of pristine MOF-carbon composite anodes for optimization PIBs. a) MOF-235 + 20 M. Reproduced with permission from Ref. [101]. Copyright (2020) Elsevier; b) Cu-HHTP/G. Reproduced with permission from Ref. [104]. Copyright (2023) Elsevier.

Table 1. Selected pristine MOF anodes for potassium-ion batteries.

MOF names	Capacity (mAh g ⁻¹ @mA g ⁻¹)	Initial Coulomb efficiency	Redox couple	Ref.
MIL-125(Ti)	208@10	58.86 %	benzene ring and carboxylate groups	[100]
MOF-235	27	45.3 %	C=O/C-O	[101]
L-Co ₂ (OH) ₂ BDC	246@100	60.65 %	Co ²⁺ /Co ⁰ and C=O/C-O	[103]
MIL-47	272@10	—	V ⁴⁺ /V ³⁺ , V ³⁺ /V ²⁺ , and C=O/C-O	[102]
Bi-MOF	415@100	38 %	Bi/BiK _x and C=O/C-O	[111]
Co ₃ [Co(CN) ₆] ₂	324.5@100	46 %	Co ³⁺ /Co ²⁺ /Co ⁺	[108]
P1-NiBTA	220@100	—	benzene ring	[106]
NiBTA	280@100	38.5 %	benzene ring	[113]
Ni-DAB	158@100	—	benzene ring	[114]
Co ₃ (HHTP) ₂	332@100	64.8 %	benzene ring	[105]
Cu-HHTP	109@100	42.62 %	benzene ring and Cu ²⁺ /Cu ⁺	[104]
HAN-Cu-MOF	455@50	42.7 %	Cu ²⁺ /Cu ⁺ and C=N/C-N	[115]
MOF-235 + 20 M	180@200	29.1 %	C=O/C-O	[101]
Cu-HHTP/G	226@100	47.68 %	benzene ring and Cu ²⁺ /Cu ⁺	[104]

performance of PIBs. Additionally, the diverse chemical compositions of unaltered MOF cathodes enable the selection of varied building units, allowing the regulation of electrochemical characteristics for flexible design and optimization of performance

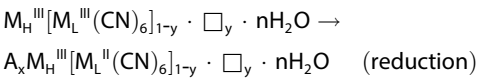
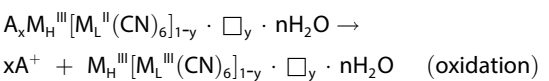
3.1. Characteristics of Pristine MOF Cathodes for PIBs

The performance of cathodes derived from pristine MOFs is significantly influenced by their characteristics in PIBs, particularly in terms of chemical-structural and micro-structural attributes. Over recent years, the commonly used MOF materials, namely PBAs and conductive π-d conjugated MOFs, have been utilized as cathodes in PIBs, achieving outstanding electrochemical performance. Among these cathodes, PBAs have been extensively investigated. PBAs are consisted of transition metal cations along with hexacyanometalate anions (such as [Fe(CN)₆]⁴⁻ and [Fe(CN)₆]³⁻) constructed with a cubic crystal structure. PBAs could show a general chemical formula of A_xM_H^{III}[M_L^{II}(CN)₆]_{1-y}·◻_y·nH₂O,^[116] where A typically representing Li, Na, or K alkali metals, M_H/M_L s denoting Fe, Co, Ni, Mn, Cu, or Zn transition metals, and ◻ signifying vacancies within PBAs. As demonstrated in Figure 5a, PBAs typically exhibit a Fm-3 m space group symmetry, in which two distinct transition metal oxidation states, i.e., high spin M_H and low spin M_L, exist. Notably, high-spin M_H is situated adjacent to N-atoms in M_HN₆ octahedra, while low-spin M_L is coordinated with C-atoms in M_LC₆ octahedra. Moreover, to maintain structural neutrality, various vacancies within PBAs are occupied by H₂O molecules and others that persist are left to accommodate varying quantities and mixed valence states between M_H and M_L.^[117] Another kind of representative cathodes for PIBs is conductive π-d conjugated MOFs, which always consist of transition metal ions (M) and organic ligands featuring O–M, S–M, and N–M

ligation sites,^[118] allowing for π electrons in a conjugated arrangement, as depicted in Figure 5b.

3.2. Potassium Storage Mechanism of Pristine MOF Cathodes for PIBs

Owing to the distinctive composition of various metal ions and ligands, the potassium storage mechanisms of pristine MOF cathodes could be elucidated through their unique chemical-structural characteristics. For instance, the energy storage mechanisms of PBA cathodes for PIBs depend on the reversible transformation among Prussian blue/Prussian white/Berlin green alongside the reversible potassium ions insertion/extraction (Figure 5a).^[119] Additionally, the discharging/charging process involves the reversible K-ions extraction/insertion, which intercalate into the Prussian blue lattice, initiating redox reactions with metal centers (e.g., Fe²⁺/Fe³⁺). The electrochemical mechanism of PBA cathodes could be explicated as follows:



Among them, the potassium storage mechanisms of conductive π-d conjugated MOF cathodes contribute to the redox reaction of transition metal ions, or the C=O/C–O, C=S/C–S, C=N/C–N redox couples (Figure 5b).

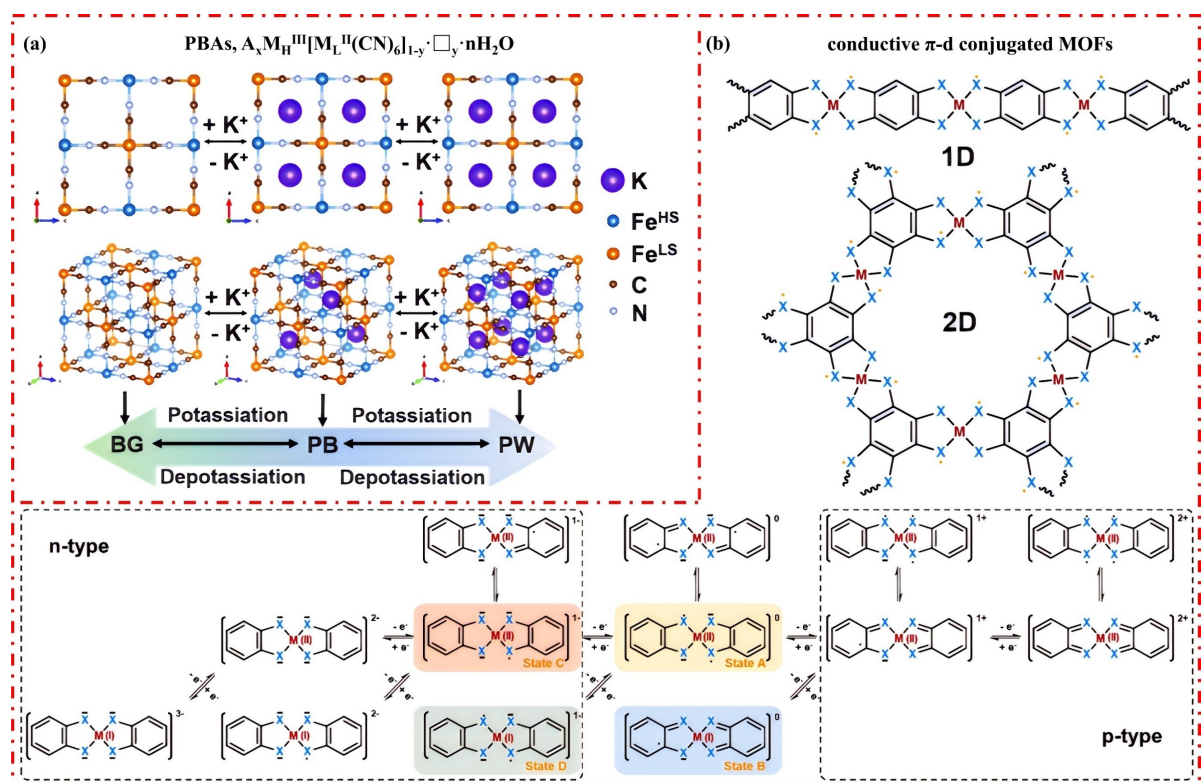


Figure 5. The characteristics of pristine MOF cathodes for PIBs. a) PBAs, $A_xM_h^{III}[M_L^{II}(CN)_6]_{1-y}\cdot\Box_y\cdot nH_2O$, Reproduced with permission from Ref. [116]. Copyright (2024) Wiley-VCH; b) conductive π -d conjugated MOFs, Reproduced with permission from Ref. [118]. Copyright (2021) American Chemical Society.

3.3. Optimization Strategies of Pristine MOF Cathodes for PIBs

The structural characteristics of MOF cathode materials, including micro- and chemical-structural aspects, play a crucial role in determining their cathode-performance in PIBs. Initially, the well-defined crystal structures and micro-pore features inherent in MOFs create optimal sites for the efficient insertion and extraction of potassium ions, thereby facilitating high-capacity energy storage. Moreover, this structural arrangement contributes to the mitigation of interactions between the electrode material and potassium ions, resulting in a reduction in internal resistance and an enhancement of energy conversion efficiency. Secondly, the chemical functional groups within MOF cathodes, specifically the choice of metal ions and variations in ligands, exert a substantial influence on the redox potential, potassium-ion diffusion kinetics, and overall stability of the cathodes. Consequently, numerous strategies have been devised in recent years to optimize the efficiency of pristine MOF cathodes and improve their properties in PIBs. These strategies encompass enhancements such as a high crystalline structure, transition metal ion doping/replacement, conductive π -d conjugated MOFs, MOF-carbon composites, and other innovative approaches.

3.3.1. High Crystalline Structure

Highly crystalline structures in pristine MOF cathodes offer a promising avenue for precise control over pore structures, facilitating unobstructed pathways for potassium ion diffusion. This serves to minimize diffusion resistance, thereby augmenting the overall electrochemical efficiency. Recent advancements in optimizing high crystalline structures have been consistently applied to enhance the electrochemical performance of PBAs for PIBs. For instance, within the realm of cathodes for PIBs, i.e., PBAs, essential factors related to the crystal structure, such as the content of crystal H_2O , A^+ , as well as $Fe(CN)_6$ vacancies, play pivotal roles in influencing the intricate electrochemical behavior. Initially, the presence of $[Fe(CN)_6]^{4-}$ vacancies impacts the content of Fe^{2+}/Fe^{3+} redox-active couple and K-ions decreasing battery capacities. Secondly, the randomly distributed vacancies are not conducive to the coordination between CN groups and transition metals, resulting in structural defects and distortions. This fragile framework cannot withstand the reversible potassium ions insertion/extraction, causing the structure to gradually collapse. Consequently, these collapsed PBAs could dissolve into the liquid electrolyte and undergo side reactions, further damaging the electrochemical properties. Finally, the crystalline H_2O molecules occupying interstitial positions impede potassium ion migration through the lattice. Reducing the content of crystalline H_2O could also potentially trigger adverse side reactions with the liquid electrolyte, posing safety concerns. Therefore, efforts must be made to minimize crystal defects and

remove crystalline H₂O during the synthesis of PBAs. A stable crystal structure is crucial not only for enhancing energy density but also for guaranteeing consistent cycling performance of PIBs. Synthesizing nearly perfect PBAs requires precise optimized synthesis parameters, e.g., the precipitation method, the synthesis temperature, and the PH value, while controlling materials' high crystallinity, minimizing crystalline H₂O, and restricting Fe(CN)₆⁴⁻ vacancies content.

For instance, via the coprecipitation method, a variety of crystal dimensions for K_{1.69}Fe[Fe(CN)₆]_{0.9}·0.4H₂O PBAs, were synthesized by Nazar and co-workers.^[120] These dimensions included nano-crystallites with a P21/n space group, sub-micron crystallites with an Fm-3 m space group, and micron crystallites with a P21/n space group, respectively. Among them, the optimal PBAs consisted of 20 nm nano-crystallites and exhibited a capacity of 140 mAh g⁻¹ within 10 mA g⁻¹. This finding underscores the crucial impact of nano-crystallite particle dimensions on the performance of potassium cathode materials. Meanwhile, Wang et al. synthesized a KFeHCF-E Fe-PBA,^[121] with ethylenediaminetetraacetic acid dipotassium salt (EDTA-2 K) serving as the chelating agent. As illustrated in Figure 6a, this synthesis occurred through a slow crystallization process, leading to enhanced crystallinity with increased K-ions content, reduced vacancies of [Fe(CN)₆]⁴⁻, and decreased crystalline H₂O content compared to KFeHCF, which was prepared without EDTA. In addition, KFeHCF-E displayed an elevated crystallinity monoclinic configuration, presenting nanoparticles with dimensions ranging from 20 to 60 nm. As a result, KFeHCF-E obtained a specific capacity of 77 mAh g⁻¹ within 25 mA g⁻¹, a commendable rate capability maintaining 60.9% capacity retention with the current densities ranging between 25 and 1000 mA g⁻¹, and an exceptional cyclability retaining 61.3% capacity after 5000 cycles with 100 mA g⁻¹. Moreover, beneficial to its high crystallinity, KFeHCF-E experienced minimal lattice change of 1.1% and cell volume expansion of 3.5% during the K-ions insertion/extraction throughout the charging and discharging

process. Moreover, EDTA-2 K could also serve as a chelating agent for Mn-Fe-based PBAs, such as K_{1.94}Mn[Fe(CN)₆]_{0.994}·□_{0.006}·0.08H₂O ingeniously devised by Zhu and collaborators.^[122] As demonstrated in Figure 6b, the as-prepared K_{1.94}Mn[Fe(CN)₆]_{0.994}·□_{0.006}·0.08H₂O manifested a commendable reversible capacity of 154.7 mAh g⁻¹, a notably elevated discharge voltage of 3.9 V vs. K⁺/K, and an impressive specific energy of 610 Wh kg⁻¹. Noteworthy is its exceptional cycling stability under 500 mA g⁻¹, attaining a capacity retention of 80% even after 7800 cycles. Meanwhile, to explore the mechanism of enduring cycling stability, measurements combining empirical studies with theoretical calculations were performed, and the results showed that the stability was due to its structurally perfect configuration and lowest water content. Thus, the utilization of the EDTA-2 K chelating agent in the preparation of PBAs resulted in twofold benefits, which not only improved the crystalline structure and morphological characteristics of PBAs but also increased the initial potassium concentration, attributing to the additional supply of K⁺ and the decreased amount of crystalline H₂O.

Moreover, synthesis temperature could be a modulating factor to optimize the electrochemical performance of MOF cathodes. For instance, by controlling the syntheses temperature of PBAs at 0 and 25 °C, Zhai et al.^[123] obtained different crystal structural PBAs with different contents of vacancy and crystalline H₂O, finding that the PB25 with fewer defects showcased outperformed cycling stability than PB0 but with a poor rate capability. Meanwhile, to investigate the influence of coordination water on the potassium storage characteristics, Jian and coworkers produced various K₂Mn[Fe(CN)₆]_n with diverse levels of coordination H₂O at different temperatures.^[124] As displayed in Figure 7a, when the reaction temperature was set at 40 °C, K₂Mn[Fe(CN)₆]₄₀ yielded the minimum concentration of coordinated H₂O and exhibited a notable capacity of 120.5 mAh g⁻¹ under 100 mA g⁻¹, accompanied by a commend-

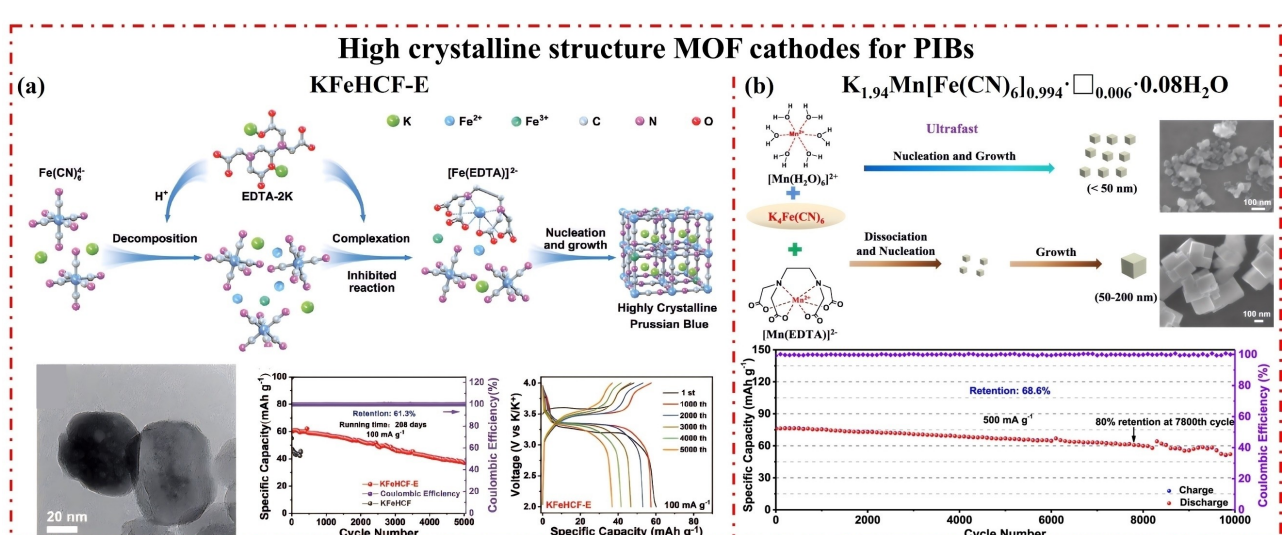


Figure 6. The structure characteristics and electrochemical performance of pristine high crystalline structure MOF cathodes with EDTA-2 K for optimization PIBs. a) KFeHCF-E. Reproduced with permission from Ref. [121]. Copyright (2023) Wiley-VCH.; b) K_{1.94}Mn[Fe(CN)₆]_{0.994}·□_{0.006}·0.08H₂O. Reproduced with permission from Ref. [122]. Copyright (2021) Springer Nature.

High crystalline structure MOF cathodes for PIBs

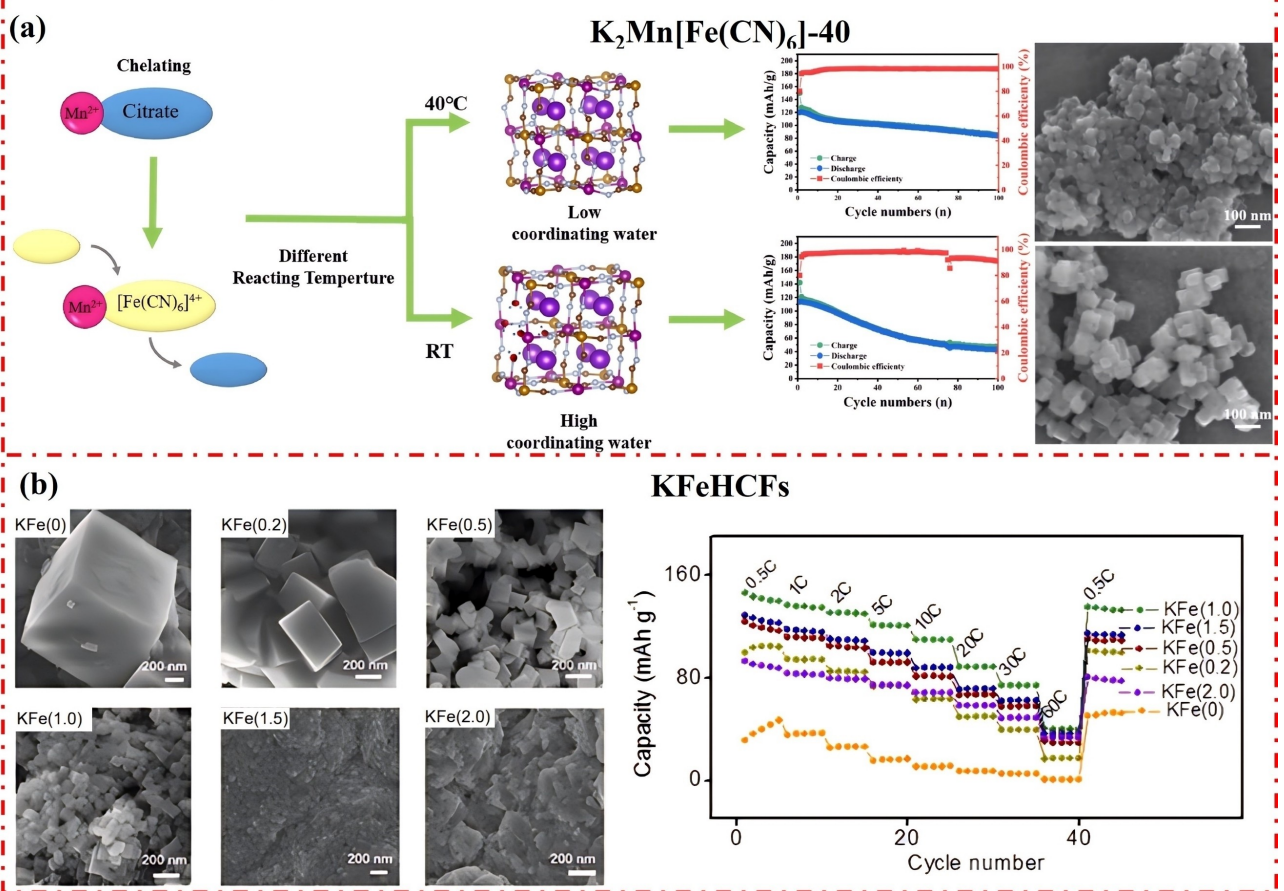


Figure 7. The structure characteristics and electrochemical performance of pristine high crystalline structure MOF cathodes for optimization PIBs by synthesis temperature or pH values. a) K₂Mn[Fe(CN)₆]-40. Reproduced with permission from Ref. [124]. Copyright (2021) Elsevier; b) KFeHCFs. Reproduced with permission from Ref. [125]. Copyright (2018) Wiley-VCH.

able rate performance, achieving 73.2 mAh g⁻¹ within 500 mAh g⁻¹.

Furthermore, the crystalline structure in PBAs for optimized electrochemical performance could be influenced not only by the precipitation method and synthesis temperature but also by pH values. For instance, to gain an optimized morphology and stoichiometry of PBAs, Li et al.^[125] modified the concentrations of HCl in the range of 0 to 2.0 mol L⁻¹, illustrating that as the HCl concentration increases, the morphology of KFeHCF transitions from approximately 1 μm well-crystallized microcuboids to about 20 nm poor-crystallized and agglomerated nanoparticles, as shown in Figure 7b. Additionally, the stoichiometry of KFeHCF initially improves before deteriorating. Notably, at HCl concentration of 1.0 mol L⁻¹, the KFeHCF sample (K_{1.93}Fe[Fe(CN)₆]_{0.97} · 1.82 H₂O, KFe(1.0)) exhibits an optimal morphology and stoichiometry, resulting in the highest capacity of 142 mAh g⁻¹ within 75 mA g⁻¹, and exceptional rate capability, achieving even 40 mAh g⁻¹ under 9000 mA g⁻¹.

3.3.2. Transition Metal Ion Doping/Replacement

In the optimization of MOF cathodes for PIBs, a pivotal strategy has arisen, involving the doping or replacement with transition metal ions. This method serves to modulate essential parameters like capacity, voltage, rate performance and economic feasibility. This strategic approach has gained significant attention due to its ability to finely adjust crucial attributes while preserving the inherent textural and compositional characteristics of the materials.

Among them, the strategy of transition metal ion doping/replacement is almost suitable for PBA cathodes due to its unique chemical structure of A_xM_H^{II}[M_L^{II}(CN)₆]_{1-y}·□_y·nH₂O, which consisting two types of transition metal ions. When employed as cathodes for PIBs, M_L usually is Fe, while M_H could be Mn, Fe, Co, Ni, Zn, or Cu, forming serval heterometallic PBAs.^[126,127] When M_H denotes a transition metal such as Ni, Zn, or Cu, which is electrochemical inertness. In these PBAs, the exclusive redox-active site is solitary the M_L^{II}, Fe²⁺, undergoing a redox reaction between Fe²⁺ and Fe³⁺ and leading to impressive cyclic disabilities and rate performance but limited

theoretical specific capacities. In contrast, if M_H represents transition metals like Mn, Fe, or Co, a dual redox-active site configuration emerges. This configuration facilitates double electron transfer reactions through both Fe^{2+}/Fe^{3+} and M^{2+}/M^{3+} redox active couples. The presence of dual redox-active sites contributes to enhanced electrochemical activity, presenting a potential advantage over the previously mentioned PBAs. As a result, these compounds may exhibit improved theoretical specific capacity compared to their counterparts with a single redox-active site. For instance, the PBA nanoparticle, $K_{1.93}Fe[Fe(CN)_6]_{0.97} \cdot 1.82H_2O$ ^[125] designed by Li et al. with $M_H=Fe$, obtaining a notable capacity of 142 mAh g^{-1} within 75 mA g^{-1} , and achieving exceptional rate capability of even 40 mAh g^{-1} under $9,000\text{ mA g}^{-1}$ contributed to the redox-active Fe^{2+}/Fe^{3+} couple. Simultaneously, Komaba and co-workers prepared $K_{1.75}Mn[Fe(CN)_6]_{0.93} \cdot 0.16H_2O$ ^[128] PBA, with $M_H=Mn$ along with fewer $[Fe(CN)_6]$ defects, exhibited a high capacity of 141 mAh g^{-1} within 30 mA g^{-1} , outstanding rate capability (108 mAh g^{-1} under $1,000\text{ mA g}^{-1}$), and excellent cycle stability involving the redox-active Fe^{2+}/Fe^{3+} and Mn^{2+}/Mn^{3+} couples, as displayed in Figure 8a. In addition, with $M_H=Mn$, Zhu et al. also delivered $K_{1.94}Mn[Fe(CN)_6]_{0.994} \cdot \square_{0.006} \cdot 0.08H_2O$ ^[122] as cathodes for PIBs, achieving a commendable reversible capacity of 154.7 mAh g^{-1} and an impressive specific energy of 609.7 Wh kg^{-1} , contributed to the redox-active Fe^{2+}/Fe^{3+} and Mn^{2+}/Mn^{3+} couples. Con-

versely, as demonstrated in Figure 8b, Cao et al. designed a $Ni-Fe$ PBA ($M_H=Ni$), $K_{1.81}Ni[Fe(CN)_6]_{0.97} \cdot 0.086H_2O$ ^[129] with minimal vacancies and reduced coordination water. With the doping of Ni, this PBA obtained a relatively lower reversible specific capacity of 57.0 mAh g^{-1} within 10 mA g^{-1} but sterling rate performance and robust cyclability due to its almost zero-strain crystal structure hinging on the redox reaction of Fe^{II}/Fe^{III} with highly reversible potassiumization and depotassiation process.

Additionally, as shown in Figure 9a, Hong et al. evaluated a $Zn-Fe$ PBA ($M_H=Zn$), $K_{1.88}Zn_{2.88}[Fe(CN)_6]_2(H_2O)_5$ ^[130] for PIBs, exhibiting an initial discharge capacity of 55.6 mAh g^{-1} within 7 mA g^{-1} and a capacity retention of 95% after 100 cycles. While with low doping content by Ni, a $Ni-Fe$ PBA, $K_2Ni_{0.05}Fe_{0.95}Fe(CN)_6$ (NiFePB-5), designed by Liao et al., gaining an elevated capacity of 135 mAh g^{-1} within 20 mA g^{-1} ^[131]. Thus, achieving comprehensive regulation of electrochemical performance necessitates appropriate control of the content of doping/replacement transition metal ions, as illustrated in Figure 9b.

3.3.3. Conductive $\pi-d$ Conjugated MOFs

As mentioned before, $\pi-d$ conjugated MOFs could also be one of the efficient optimization methods to utilize advanced cathodes for PIBs with excellent electrochemical performance,

Transition metal ion doping/replacement MOF cathodes for PIBs

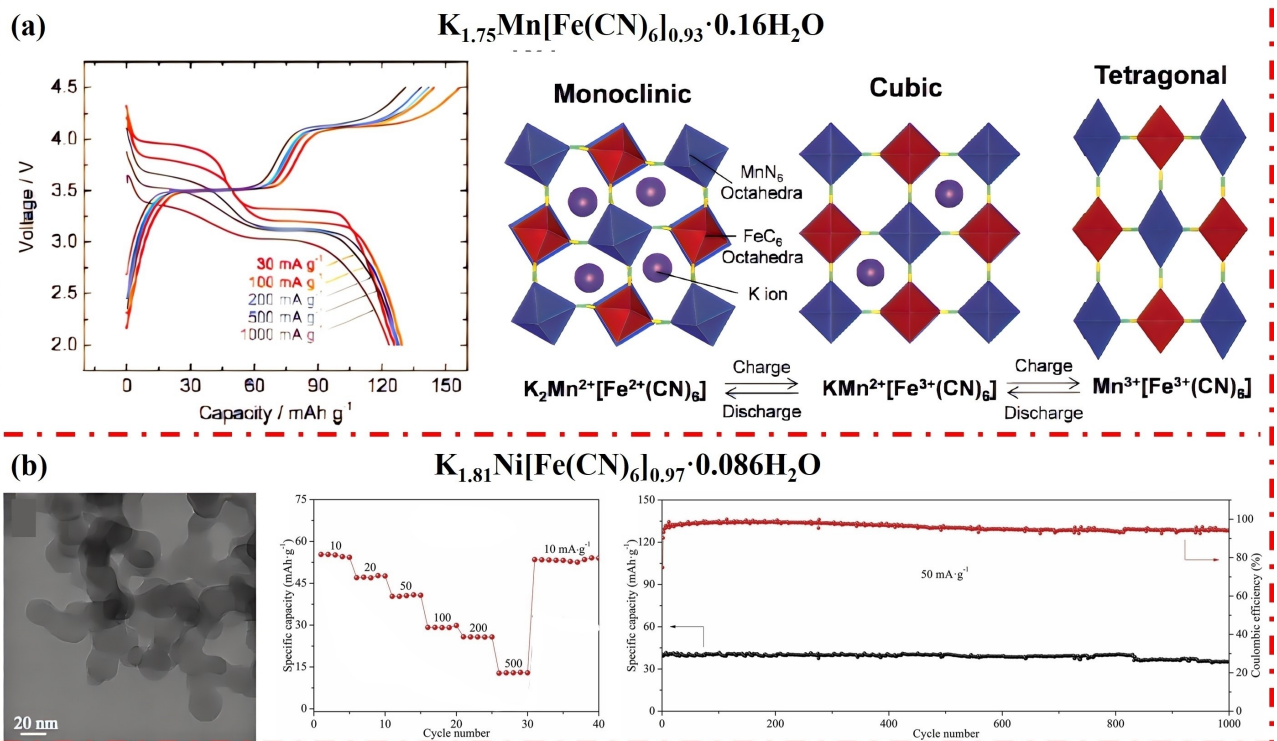


Figure 8. The structure characteristics and electrochemical performance of pristine transition metal ion doping/replacement MOF cathodes for optimization PIBs. a) $K_{1.75}Mn[Fe(CN)_6]_{0.93} \cdot 0.16H_2O$. Reproduced with permission from Ref. [128]. Copyright (2012) Royal Society of Chemistry; b) $K_{1.81}Ni[Fe(CN)_6]_{0.97} \cdot 0.086H_2O$. Reproduced with permission from Ref. [129]. Copyright (2019) Wiley-VCH; c) $K_{1.88}Zn_{2.88}[Fe(CN)_6]_2(H_2O)_5$, Reproduced with permission from Ref. [130]. Copyright (2019) American Chemical Society; d) $K_2Ni_{0.05}Fe_{0.95}Fe(CN)_6$ (NiFePB-5). Reproduced with permission from Ref. [131]. Copyright (2019) American Chemical Society.

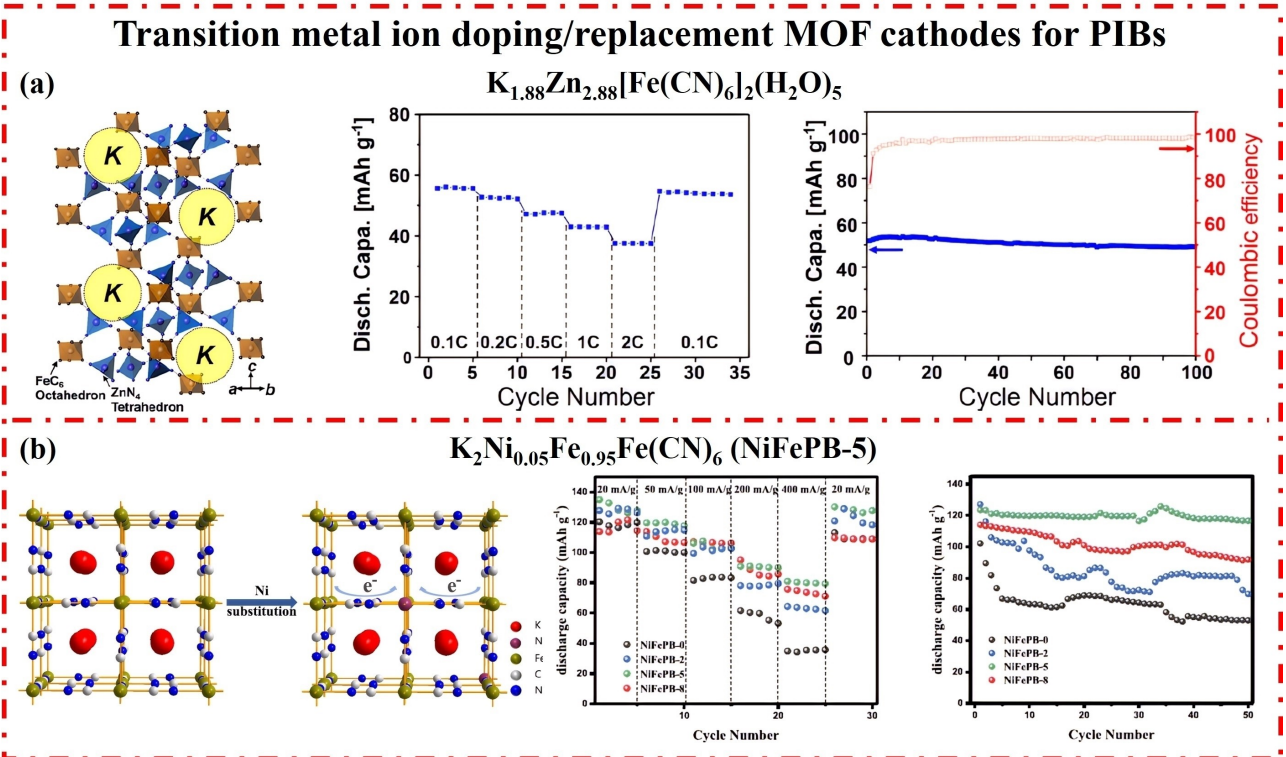


Figure 9. The structure characteristics and electrochemical performance of pristine transition metal ion doping/replacement MOF cathodes for optimization PIBs. a) $K_{1.88}Zn_{2.88}[Fe(CN)_6]_2(H_2O)_5$, Reproduced with permission from Ref. [130]. Copyright (2019) American Chemical Society; b) $K_2Ni_{0.05}Fe_{0.95}Fe(CN)_6$ (NiFePB-5). Reproduced with permission from Ref. [131]. Copyright (2019) American Chemical Society.

thanks to the advantages of improved conductivity and natural structure.

For instance, the Ni-TTO π -d conjugated MOF was synthesized by Kapaev et al.^[132] and subsequently employed as cathodes for PIBs with commendable conductivity ($>1\text{ S cm}^{-1}$). As shown in Figure 10a, operating within the voltage range of 1.5 V to 3.6 V vs. K^+/K , Ni-TTO demonstrated a capacity of 209 mAh g^{-1} within 100 mA g^{-1} , showcasing a two-electron redox reaction attributed to the redox-active C=S/C–S couple. After that, π -d conjugated Cu-MOFs have also emerged as novel cathodes for PIBs. For example, Zhu et al. demonstrated a hexaazanonaphthalene (HATN)-based π -d conjugated MOF, Cu-HATNH, as cathodes for PIBs.^[133] As displayed in Figure 10b, Cu-HATNH exhibited spherical morphology, however, obtaining a relatively lower capacity of approximately 100 mAh g^{-1} within 100 mA g^{-1} and exhibiting poor long-cycle and rate performance despite the multi-electron redox-active $[CuO_4]$ units. To further enhance the conductivity of π -d conjugated Cu-HATNH cathodes, a hybrid material, Cu-HATNH@CNT, was synthesized by employing a controllable in-situ growth strategy to integrate carbon nanotubes (CNTs). As expected, Cu-HATNH@CNT demonstrated promising characteristics, including a high initial capacity of 317.5 mAh g^{-1} within 100 mA g^{-1} , remarkable long-term cycling stability (96.8% capacity retention under $5,000\text{ mA g}^{-1}$ after 2200 cycles), and exceptional rate capacity (147.1 mAh g^{-1} under $10,000\text{ mA g}^{-1}$). The potassium-ion storage mechanism for Cu-HATNH involved dissecting the redox-active Cu^{2+}/Cu^+ , $C=O/C–O$, and $C=N/C–N$ couples within

$[CuO_4]$ units through a combination of experimental characterization and density functional theory calculations in the utilization as anodes for PIBs, the pristine MOFs typically exhibit a configuration consisting of metal.

3.3.4. MOF-carbon Composites

MOF-carbon composites present notable advantages, including further increased surface areas, improved electrochemical stability, and enhanced potassium-ion transport kinetics, and enabling fast potassiumization and depotassification processes, as cathodes for optimized PIBs with enhanced electrochemical performance. Recently, the MOF-carbon composites usually consist of conductive carbon (C), multi-walled carbon nanotubes (CNTs), graphene (G), or reduced graphene oxide (rGO).

For instance, composites of $K_4Fe(CN)_6/C$ were fabricated by employing the ball-milling technique, offering an economical choice for cathodes in PIBs by Li and coworkers.^[134] As demonstrated in Figure 11a, $K_4Fe(CN)_6/C$ obtained a high redox voltage of approximately 3.6 V and a discharge capacity of 65.5 mAh g^{-1} with 20 mA g^{-1} , maintaining stable performance over 400 cycles with an average capacity degradation of 0.063% per cycle. This enhanced cycling stability can be ascribed to the highly reversible redox pair of $[Fe(CN)_6]^{3-/-4-}$, along with the reduction in particle size and enhancement in ionic and electronic conductivity after ball milling with carbon. Potassium-ion storage mechanism analysis indicates that the

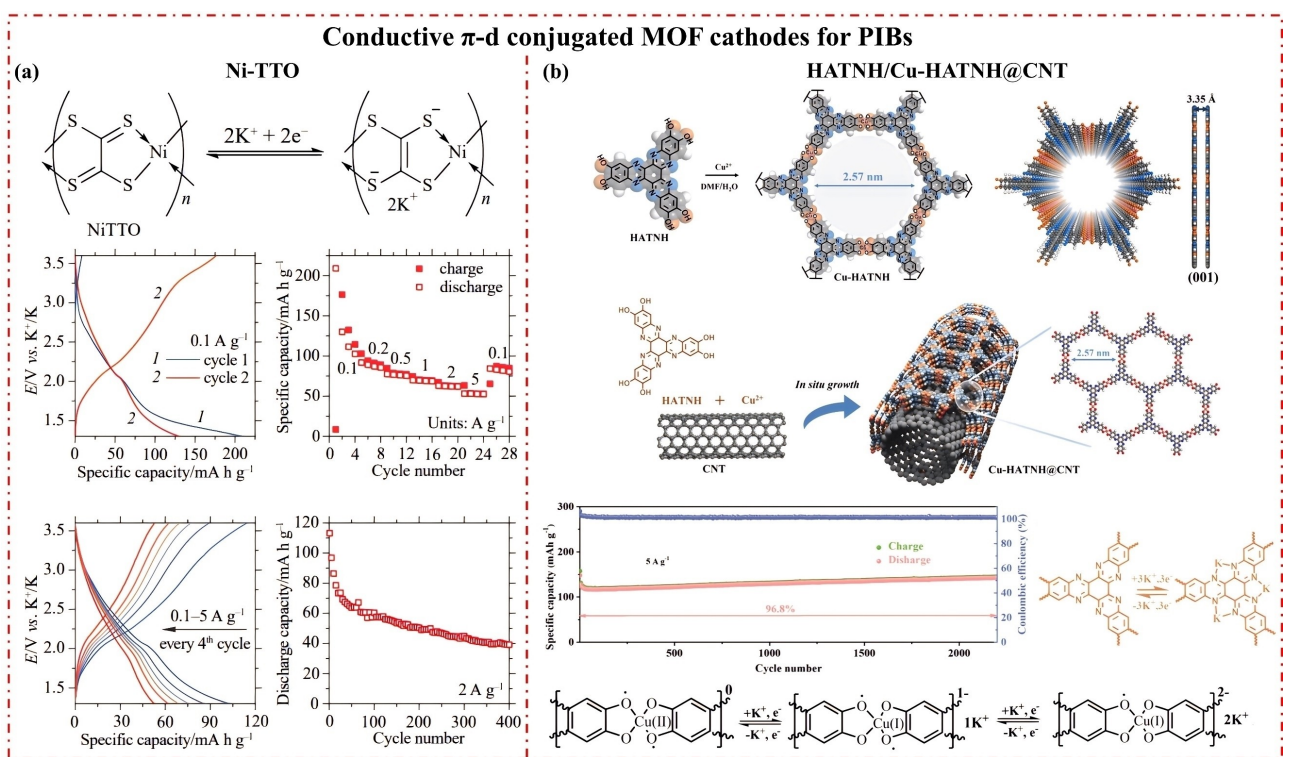


Figure 10. The structure characteristics and electrochemical performance of pristine conductive π -d conjugated MOF cathodes for optimization PIBs. a) Ni-TTO. Reproduced with permission from Ref. [132]. Copyright (2022) Elsevier; b) Cu-HATNH/Cu-HATNH@CNT. Reproduced with permission from Ref. [133]. Copyright (2023) Wiley-VCH.

$\text{K}_4\text{Fe}(\text{CN})_6$ electrode undergoes a one-electron transfer process, facilitating the valence transition of Fe between Fe^{2+} and Fe^{3+} to maintain charge equilibrium. Meanwhile, a π -d conjugated hybrid material, Cu-HATNH@CNT, was engineered by synthesizing Cu-HATNH on CNTs through an in-situ growth approach by Zhu et al.^[133] Cu-HATNH@CNT showcased a core-shell structure, effectively mitigating π - π layer accumulation interactions and shortening the diffusion pathway of K-ions, thereby enabling efficient reversible K^+ storage. As anticipated, Cu-HATNH@CNT demonstrated an initial capacity of 318 mAh g^{-1} within 100 mA g^{-1} , maintained 96.8% capacity retention at $5,000 \text{ A g}^{-1}$ after 2200 cycles, and achieved a capacity of 147.1 mAh g^{-1} under $10,000 \text{ A g}^{-1}$.

Moreover, serving as a substrate, graphene (G) found utility in PBAs. As shown in Figure 11b, $\text{K}_{1.85}\text{Mn}[\text{Fe}(\text{CN})_6]_{0.98} \cdot \square_{0.02} \cdot 7\text{H}_2\text{O}$ -graphene(KPB/G)^[135] nanocomposite was achieved by combining KPB with graphene in ball-milling method. Through ball milling with few-layered graphene, the pristine KPB particles, ranging from 100 to 200 nm, underwent fragmentation into smaller grains measuring 40–80 nm, which are uniformly affixed to the conductive graphene surface. Contrasting with the pristine KPB sample, the KPB/G composite showcased a superior capacity of 131.4 mAh g^{-1} within 0.1 C, a markedly improved rate capability with 108.8 mAh g^{-1} within 5 C and 100.2 mAh g^{-1} within 10 C, and extended cycling performance with maintaining 96.9% capacity after 120 cycles under 0.5 C, 89.3% capacity after 500 cycles under 5 C, and 82.4% capacity after 300 cycles under 10 C, respectively. In

addition, Zhu et al. devised a composite of $\text{K}_{1.91}\text{Mn}[\text{Fe}(\text{CN})_6]_{0.965} \cdot \square_{0.035} \cdot 0.389\text{H}_2\text{O}$ -reduced graphene oxide (KMF-RGO) by ball milling KMF with RGO (wt.% of KMF:RGO = 7:1) possessing a large surface area and high electrical conductivity.^[136] As demonstrated in Figure 11c, KMF-RGO manifested outstanding cycling stability (0.62 mAh cm^{-2} , i.e., 151.8 mAh g^{-1} within 15 mA g^{-1} for 100 cycles), alongside rapid rate capability (0.24 mAh cm^{-2} , i.e., 58.8 mAh g^{-1} within 450 mA g^{-1}), and remarkable air stability, maintaining electrochemical performance even after 30 days in a standard indoor atmosphere, attributed to the exceptional structural integrity of KMF, which featuring an extremely low defect content rendering them less vulnerable to oxidation and moisture exposure.

In conclusion, enhancing the electrochemical performance of PIB cathodes through optimization strategies remains a crucial endeavor in the field of electrochemical energy storage. Enhancing the crystallinity of MOF cathode architecture is a fundamental approach to promote efficient pathways for charge transfer and ensure structural robustness during electrochemical processes. Incorporating transition metal-ion doping or substitution serves to finely tune the electronic structure and redox characteristics of MOFs, thus elevating their specific capacity and cycling durability. Moreover, the amalgamation of conductive π -d conjugated MOFs exploits synergistic interactions between organic ligands and metal cores, facilitating electron transfer kinetics and overall conductivity. Introducing composite materials comprising MOFs and carbonaceous substrates further augments electrode conductivity and structural

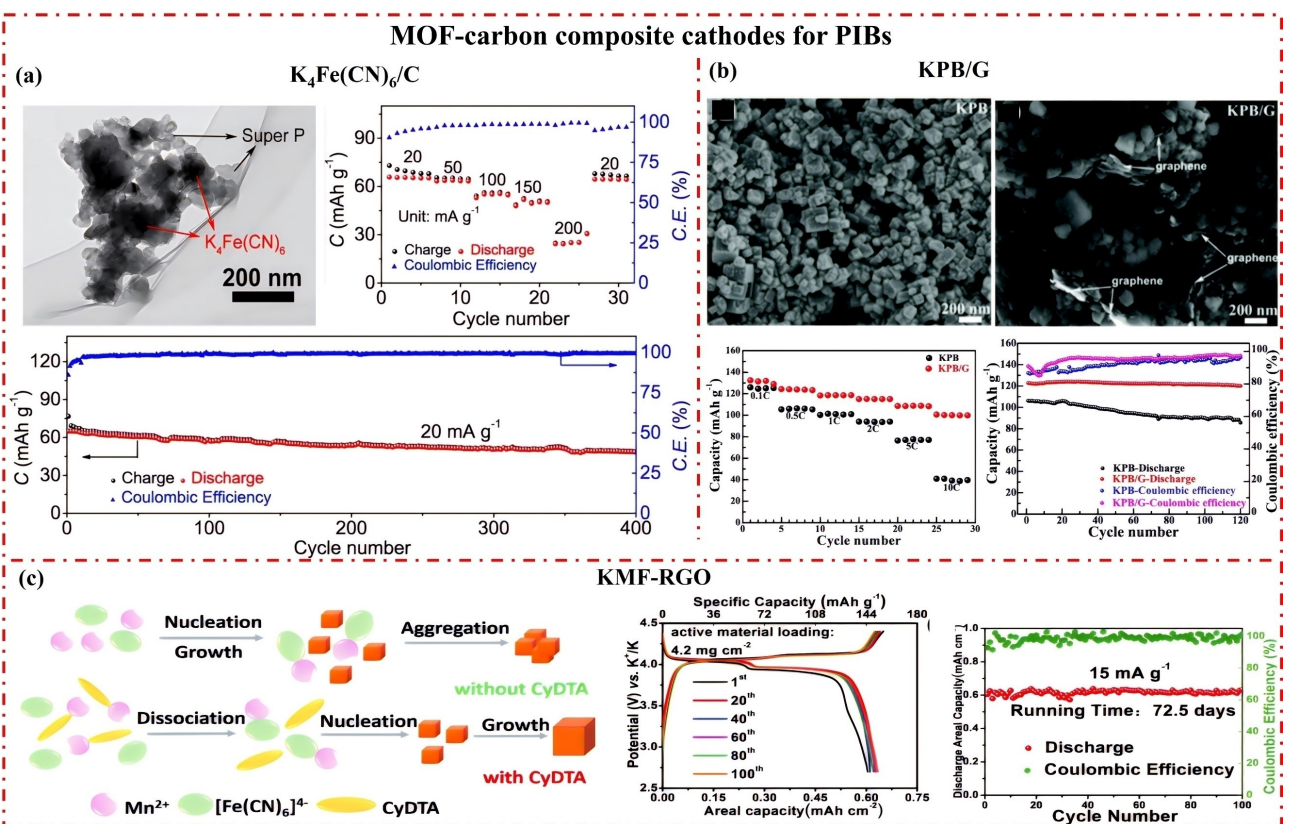


Figure 11. The structure characteristics and electrochemical performance of pristine MOF-carbon composite cathodes for optimization PIBs. a) $K_4Fe(CN)_6/C$. Reproduced with permission from Ref. [134]. Copyright (2018) Wiley-VCH; b) $K_{1.85}Mn[Fe(CN)_6]_{0.98}\square_{0.02}\cdot7H_2O$ -graphene(KPB/G). Reproduced with permission from Ref. [135]. Copyright (2019) Royal Society of Chemistry; c) $K_{1.91}Mn[Fe(CN)_6]_{0.965}\square_{0.035}\cdot0.389H_2O$ -reduced graphene oxide (KMF-RGO). Reproduced with permission from Ref. [136]. Copyright (2021) Royal Society of Chemistry.

resilience, mitigating volume expansion issues during PIB operation. By adeptly amalgamating these methodologies, pivotal challenges associated with PIB cathodes—such as low conductivity, restricted ion diffusion kinetics, and subpar cycling stability—are effectively addressed. The electrochemical properties of recent MOF cathodes for PIBs are shown in Table 2.

4. Summary and Outlook

Pristine MOF electrodes, no matter cathodes or anodes, have been utilized as promising electrodes for novel electrochemical energy storage devices, especially in PIBs, thanks to their natural characteristics along with advanced optimized strategies, including enhancing high crystalline structure, designing high-conductive π -d conjugated MOFs, preparing MOF/composites, and so on. However, upon closer scrutiny of recent investigations centered on pristine electrodes composed of MOFs, various hurdles emerge that require attention: 1) Structural Stability: During the potassiumization and deprotonation process, the larger ionic radius of potassium-ions, the structural properties of MOFs, as well as electrolyte solvent selectivity, could influence the dynamic nature of MOF frameworks, leading to undesired structural degradation, limiting the overall cycling stability and performance; 2) Low Electrical

Conductivity and Kinetic Limitations: Inherent low electrical conductivity and kinetic limitations of certain MOF materials hinders efficient charge transport and potassium-ion transport within the electrode, resulting in poor rate capability and overall electrochemical performance in PIBs; 3) Capacity decay and cycle stability: The irreversible chemical reactions or the limited diffusion of potassium-ions between potassium-ions and functional groups within MOFs during PIBs operation, leading to the MOF electrodes may encounter issues such as capacity decay and degradation of electrochemical performance and resulting in decreased battery performance.

Notwithstanding these challenges, pristine MOF electrodes hold substantial promise for employment in PIBs, particularly after optimization. To unleash the complete potential of MOFs for PIBs, a range of strategies ought to be advanced to surmount these impediments: 1) Conductivity Enhancement: Strategies to improve the electrical conductivity of MOFs include doping with conductive materials (such as G/CNTs/RGO), creating hybrid structures, or utilizing conductive π -d conjugated MOFs. These approaches facilitate efficient charge transport and enhance overall electrochemical performance; 2) Material Design and Engineering: Tailoring the design and engineering of MOF cathodes, such as the chemical composition, pore size, and surface functionality, could enhance their electrochemical stability, conductivity, and ion diffusion kinetics.

Table 2. Selected pristine MOF cathodes for Potassium-ion batteries.

MOF names	MOF types	Capacity (mAh g ⁻¹ @mA g ⁻¹)	Redox couple	Potential (V)	Ref.
K _{1.69} Fe[Fe(CN) ₆] _{0.9} ·0.4H ₂ O	PBAs	140@10	Fe ²⁺ /Fe ³⁺	2.0-4.6	[120]
KFeHCF-E	PBAs	77@25	Fe ²⁺ /Fe ³⁺	2.0-4.0	[121]
KFe ^{III} [Fe ^{II} (CN) ₆]	PBAs	78@0.1 C	Fe ²⁺ /Fe ³⁺	2.7-4.2	[137]
K _{0.220} Fe[Fe(CN) ₆] _{0.805} ·□ _{0.195} ·4.01H ₂ O	PBAs	76.7@50	Fe ²⁺ /Fe ³⁺	2.0-4.0	[138]
K ₂ Fe ^{II} [Fe ^{II} (CN) ₆]·2H ₂ O	PBAs	120@200	Fe ²⁺ /Fe ³⁺	3.0-4.2	[139]
K ₂ Fe[Fe(CN) ₆]	PBAs	60@100	Fe ²⁺ /Fe ³⁺	2.0-4.0	[140]
K _{1.93} Fe[Fe(CN) ₆] _{0.97} ·1.82H ₂ O	PBAs	142@75	Fe ²⁺ /Fe ³⁺	-	[125]
K _{0.220} Fe[Fe(CN) ₆] _{0.805} ·4.01H ₂ O	PBAs	73.2@50	Fe ²⁺ /Fe ³⁺	2-4	[138]
K _{1.68} Fe _{1.09} Fe(CN) ₆ ·2.1H ₂ O	PBAs	110@20	Fe ²⁺ /Fe ³⁺	2-4.5	[141]
K _{1.69} Fe[Fe(CN) ₆] _{0.90} ·0.4H ₂ O	PBAs	140@10	Fe ²⁺ /Fe ³⁺	2-4.5	[120]
K _{1.92} Fe[Fe(CN) ₆] _{0.94} ·0.5H ₂ O	PBAs	133@13	Fe ²⁺ /Fe ³⁺	2-4.25	[142]
K _{1.62} Fe[Fe(CN) ₆] _{0.92} ·0.33H ₂ O	PBAs	120.9@50	Fe ²⁺ /Fe ³⁺	2.5-4.5	[143]
K _{1.56} Fe[Fe(CN) ₆] _{0.89} ·1.86H ₂ O	PBAs	118@77.5	Fe ²⁺ /Fe ³⁺	2-4.4	[144]
K _{1.43} Fe[Fe(CN) ₆] _{0.94} ·0.42H ₂ O	PBAs	110@50	Fe ²⁺ /Fe ³⁺	2.5-4.3	[123]
K ₄ Fe(CN) ₆ ·C	PBAs	65.5@20	Fe ²⁺ /Fe ³⁺	2.0-4.0	[134]
K _{1.89} Mn[Fe(CN) ₆] _{0.92} ·0.75H ₂ O	PBAs	142.4@28	Fe ²⁺ /Fe ³⁺ and Mn ²⁺ /Mn ³⁺	2.5-4.5	[145]
K _{1.85} Mn[Fe(CN) ₆] _{0.91} ·0.65H ₂ O	PBAs	104.8@20	Fe ²⁺ /Fe ³⁺ and Mn ²⁺ /Mn ³⁺	2-4.5	[146]
K _{1.94} Mn[Fe(CN) ₆] _{0.994} ·□ _{0.006} ·0.08H ₂ O	PBAs	154.7@15	Fe ²⁺ /Fe ³⁺ and Mn ²⁺ /Mn ³⁺	2.7-4.4	[122]
K _{1.75} Mn[Fe(CN) ₆] _{0.93} ·0.16H ₂ O	PBAs	141@30	Fe ²⁺ /Fe ³⁺ and Mn ²⁺ /Mn ³⁺	2.0-4.5	[128]
K ₂ Mn[Fe(CN) ₆]·40	PBAs	120.5@100	Fe ²⁺ /Fe ³⁺ and Mn ²⁺ /Mn ³⁺	2.5-4.5	[124]
K _{1.85} Mn[Fe(CN) ₆] _{0.98} ·□ _{0.02} ·7H ₂ O-G	PBAs	131.4@0.1 C	Fe ²⁺ /Fe ³⁺ and Mn ²⁺ /Mn ³⁺	2.0-4.4	[135]
K _{1.91} Mn[Fe(CN) ₆] _{0.965} ·□ _{0.035} ·0.389H ₂ O-RGO	PBAs	151.8@15	Fe ²⁺ /Fe ³⁺ and Mn ²⁺ /Mn ³⁺	2.7-4.4	[136]
K _{1.55} Co _{0.88} Fe(CN) ₆ ·3.2H ₂ O	PBAs	60@20	Co ³⁺ /Co ²⁺ and Fe ³⁺ /Fe ²⁺	2.0-4.2	[141]
K _{0.6} Ni _{1.2} Fe(CN) ₆ ·3.6H ₂ O	PBAs	59@50	Fe ²⁺ /Fe ³⁺	3.1-3.7	[147]
K ₂ Ni _{0.05} Fe _{0.95} Fe(CN) ₆	PBAs	135@20	Fe ²⁺ /Fe ³⁺	2.0-4.5	[131]
K _{1.81} Ni[Fe(CN) ₆] _{0.97} ·0.086H ₂ O	PBAs	57@10	Fe ²⁺ /Fe ³⁺	2.0-4.5	[129]
K _{1.88} Zn _{2.88} [Fe(CN) ₆] ₂ (H ₂ O) ₅	PBAs	55.6@7	Fe ²⁺ /Fe ³⁺	3.2-4.1	[130]
K ₂ Ni _x Co _{1-x} Fe(CN) ₆	PBAs	86@20	Co ³⁺ /Co ²⁺ and Fe ³⁺ /Fe ²⁺	2.0-4.5	[148]
K _{1.69} Mn _{0.779} Ni _{0.221} [Fe(CN) ₆] _{0.93} ·0.392H ₂ O	PBAs	130.6@10	Fe ²⁺ /Fe ³⁺ and Mn ²⁺ /Mn ³⁺	2-4.5	[149]
Ni-TTO	π-d	209@100	C=S/C-S	1.5-3.6	[132]
Cu-HATNH	π-d	100@100	Cu ²⁺ /Cu ⁺ , C=O/C—O, and C=N/C-N	1.0-3.5	[133]
Cu-HATNH@CNT		317.5@100			

Strategies such as functionalization with redox-active groups, surface engineering techniques, and engineering hierarchical architectures can mitigate the aforementioned challenges; 3) Nano-structuring and Composite Formation: Incorporating MOF nanoparticles into conductive matrices or forming hybrid composites with carbonaceous materials (e.g., graphene, carbon nanotubes) can improve the overall conductivity, mechanical stability, specific surface area, and electrochemical performance of MOF-based electrodes.

The utilization of MOF materials as electrode materials for PIBs presents significant opportunities for advancing electrochemical energy storage technologies. Overcoming current challenges to fully harness the potential of MOF-based electrodes is paramount, necessitating enhancements in electrical conductivity, chemical composition design, structural engineering, and nanotechnology. Future research endeavors should

prioritize the exploration of novel MOF materials, employ advanced structural characterization and mechanistic analysis techniques, integrate MOFs into composite structures, and foster interdisciplinary collaboration to propel the development of high-performance potassium-ion batteries.

Acknowledgements

This work was supported by the Foundation of Sichuan University of Science & Engineering (2023RC02, 2023RC03). K.W. thanks the National Natural Science Foundation of China (22279061) and the Natural Science Foundation of Jiangsu Province (BK20180514).

Conflict of Interests

The authors declare no conflict of interest.

Keywords: potassium-ion batteries · MOFs · anodes · cathodes

- [1] X. Wang, Z. Xiao, K. Han, X. Zhang, Z. Liu, C. Yang, J. Meng, M. Li, M. Huang, X. Wei, *Adv. Energy Mater.* **2023**, *13*, 2202861.
- [2] J. Zheng, C. Hu, L. Nie, H. Chen, S. Zang, M. Ma, Q. Lai, *Advanced Materials Technologies* **2023**, *8*, 2201591.
- [3] W. Zhang, R. Huang, X. Yan, C. Tian, Y. Xiao, Z. Lin, L. Dai, Z. Guo, L. Chai, *Angew. Chem. Int. Ed.* **2023**, *62*, e202308891.
- [4] J. Hu, Y. Hong, M. Guo, Y. Hu, W. Tang, S. Xu, S. Jia, B. Wei, S. Liu, C. Fan, *Energy Storage Mater.* **2022**, *52*, 61–68.
- [5] X. Tang, C. Liu, H. Wang, L.-P. Lv, W. Sun, Y. Wang, *Coord. Chem. Rev.* **2023**, *494*, 215361.
- [6] L. Ma, Y. Lv, J. Wu, C. Xia, Q. Kang, Y. Zhang, H. Liang, Z. Jin, *Nano Res.* **2021**, *14*, 4442–4470.
- [7] C. Li, Y. Yuan, M. Yue, Q. Hu, X. Ren, B. Pan, C. Zhang, K. Wang, Q. Zhang, *Small* **2024**, *20*, 2310373.
- [8] T. Naren, R. Jiang, Q. Gu, G.-C. Kuang, L. Chen, Q. Zhang, *Mater. Today Energy* **2024**, *40*, 101512.
- [9] S. Xu, C. Wang, T. Song, H. Yao, J. Yang, X. Wang, J. Zhu, C. S. Lee, Q. Zhang, *Adv. Sci.* **2023**, *10*, 2304497.
- [10] C. Li, C. Zhang, K. Wang, F. Yu, J. Xie, Q. Zhang, *Chem. Eng. J.* **2022**, *431*, 133234.
- [11] M. Sha, L. Liu, H. Zhao, Y. Lei, *Energy Environ. Mater.* **2020**, *3*, 56–66.
- [12] Y. Wu, H. Zhao, Z. Wu, L. Yue, J. Liang, Q. Liu, Y. Luo, S. Gao, S. Lu, G. Chen, *Energy Storage Mater.* **2021**, *34*, 483–507.
- [13] Q. Pan, Z. Tong, Y. Su, S. Qin, Y. Tang, *Adv. Funct. Mater.* **2021**, *31*, 2103912.
- [14] L. Fan, Y. Hu, A. M. Rao, J. Zhou, Z. Hou, C. Wang, B. Lu, *Small Methods* **2021**, *5*, 2101131.
- [15] X. Min, J. Xiao, M. Fang, W. A. Wang, Y. Zhao, Y. Liu, A. M. Abdelkader, K. Xi, R. V. Kumar, Z. Huang, *Energy Environ. Sci.* **2021**, *14*, 2186–2243.
- [16] W. Zhang, H. Sun, P. Hu, W. Huang, Q. Zhang, *EcoMat* **2021**, *3*, e12128.
- [17] W. Zhang, W. Huang, Q. Zhang, *Chemistry—A European Journal* **2021**, *27*, 6131–6144.
- [18] J. Xie, Q. Zhang, *Mater. Today Energy* **2020**, *18*, 100547.
- [19] M. Eddaoudi, J. Kim, N. Rosi, D. Vodak, J. Wachter, M. O’Keeffe, O. M. Yaghi, *Science* **2002**, *295*, 469–472.
- [20] J. Gao, M. He, Z. Y. Lee, W. Cao, W.-W. Xiong, Y. Li, R. Ganguly, T. Wu, Q. Zhang, *Dalton Trans.* **2013**, *42*, 11367–11370.
- [21] J. Gao, K. Ye, M. He, W.-W. Xiong, W. Cao, Z. Y. Lee, Y. Wang, T. Wu, F. Huo, X. Liu, *J. Solid State Chem.* **2013**, *206*, 27–31.
- [22] Y.-P. Wu, X.-Q. Wu, J.-F. Wang, J. Zhao, W.-W. Dong, D.-S. Li, Q.-C. Zhang, *Cryst. Growth Des.* **2016**, *16*, 2309–2316.
- [23] G. W. Xu, Y. P. Wu, W. W. Dong, J. Zhao, X. Q. Wu, D. S. Li, Q. Zhang, *Small* **2017**, *13*, 1602996.
- [24] P. Li, F.-F. Cheng, W.-W. Xiong, Q. Zhang, *Inorg. Chem. Front.* **2018**, *5*, 2693–2708.
- [25] Z.-S. Qin, W.-W. Dong, J. Zhao, Y.-P. Wu, Q. Zhang, D.-S. Li, *Inorg. Chem. Front.* **2018**, *5*, 120–126.
- [26] J. Zhao, X. Liu, Y. Wu, D.-S. Li, Q. Zhang, *Coord. Chem. Rev.* **2019**, *391*, 30–43.
- [27] C. Li, K. Wang, J. Li, Q. Zhang, *Nanoscale* **2020**, *12*, 7870–7874.
- [28] K. Wang, X. Shi, Z. Zhang, X. Ma, Y. Lu, H. Wang, *J. Alloys Compd.* **2015**, *632*, 361–367.
- [29] A. Dhakshinamoorthy, A. M. Asiri, H. Garcia, *Angew. Chem. Int. Ed.* **2016**, *55*, 5414–5445.
- [30] X. Cao, C. Tan, M. Sindoro, H. Zhang, *Chem. Soc. Rev.* **2017**, *46*, 2660–2677.
- [31] B. Ghalei, K. Sakurai, Y. Kinoshita, K. Wakimoto, A. P. Isfahani, Q. Song, K. Doitomi, S. Furukawa, H. Hirao, H. Kusuda, *Nat. Energy* **2017**, *2*, 17086.
- [32] X. Lian, Y. Fang, E. Joseph, Q. Wang, J. Li, S. Banerjee, C. Lollar, X. Wang, H.-C. Zhou, *Chem. Soc. Rev.* **2017**, *46*, 3386–3401.
- [33] Z. Kang, L. Fan, D. Sun, *J. Mater. Chem. A* **2017**, *5*, 10073–10091.
- [34] J. Liu, D. Zhu, C. Guo, A. Vasileff, S. Z. Qiao, *Adv. Energy Mater.* **2017**, *7*, 1700518.
- [35] M. X. Wu, Y. W. Yang, *Adv. Mater.* **2017**, *29*, 1606134.
- [36] C. Li, H. Tan, J. Pei, C. Wang, C. Fan, F. Huang, B. Cao, M. Hao, Y. Li, Z. Wang, J. Li, *New J. Chem.* **2017**, *41*, 14539–14544.
- [37] K.-B. Wang, Q. Xun, Q. Zhang, *EnergyChem* **2020**, *2*, 100025.
- [38] O. M. Yaghi, G. Li, H. Li, *Nature* **1995**, *378*, 703–706.
- [39] W. Fan, X. Zhang, Z. Kang, X. Liu, D. Sun, *Coord. Chem. Rev.* **2021**, *443*, 213968.
- [40] H. Li, L. Li, R.-B. Lin, W. Zhou, Z. Zhang, S. Xiang, B. Chen, *EnergyChem* **2019**, *1*, 100006.
- [41] H. Daglar, H. C. Gulbalkan, G. Avci, G. O. Aksu, O. F. Altintas, I. Erucar, S. Keskin, *Angew. Chem. Int. Ed.* **2021**, *60*, 7828–7837.
- [42] D.-X. Xue, Q. Wang, J. Bai, *Coord. Chem. Rev.* **2019**, *378*, 2–16.
- [43] L.-F. Ma, D.-S. Li, G.-P. Yang, Q. Zhang, *Front. Chem.* **2023**, *11*, 1245159.
- [44] Y. Shen, T. Pan, L. Wang, Z. Ren, W. Zhang, F. Huo, *Adv. Mater.* **2021**, *33*, 2007442.
- [45] T. A. Goetjen, J. Liu, Y. Wu, J. Sui, X. Zhang, J. T. Hupp, O. K. Farha, *Chem. Commun.* **2020**, *56*, 10409–10418.
- [46] M. Ali, E. Pervaiz, T. Noor, O. Rabi, R. Zahra, M. Yang, *Int. J. Energy Res.* **2021**, *45*, 1190–1226.
- [47] T. Zhao, H. Wu, X. Wen, J. Zhang, H. Tang, Y. Deng, S. Liao, X. Tian, *Coord. Chem. Rev.* **2022**, *468*, 214642.
- [48] V. Shrivastav, S. Sundriyal, P. Goel, H. Kaur, S. K. Tuteja, K. Vikrant, K.-H. Kim, U. K. Tiwari, A. Deep, *Coord. Chem. Rev.* **2019**, *393*, 48–78.
- [49] D. Vallejo-Sánchez, P. Amo-Ochoa, G. Beobide, O. Castillo, M. Fröba, F. Hoffmann, A. Luque, P. Ocón, S. Pérez-Yáñez, *Adv. Funct. Mater.* **2017**, *27*, 1605448.
- [50] E. A. Dolgopolova, A. M. Rice, C. R. Martin, N. B. Shustova, *Chem. Soc. Rev.* **2018**, *47*, 4710–4728.
- [51] Q. Ren, H. Wang, X. F. Lu, Y. X. Tong, G. R. Li, *Adv. Sci.* **2018**, *5*, 1700515.
- [52] L. Yang, X. Zeng, W. Wang, D. Cao, *Adv. Funct. Mater.* **2018**, *28*, 1704537.
- [53] B. Gui, Y. Meng, Y. Xie, J. Tian, G. Yu, W. Zeng, G. Zhang, S. Gong, C. Yang, D. Zhang, C. Wang, *Adv. Mater.* **2018**, *30*, 1802329.
- [54] K. Wang, X. Cao, S. Wang, W. Zhao, J. Xu, Z. Wang, H. Wu, *ACS Appl. Mater. Interfaces* **2018**, *10*, 9104–9115.
- [55] L. Wang, H. Xu, J. Gao, J. Yao, Q. Zhang, *Coord. Chem. Rev.* **2019**, *398*, 213016.
- [56] Z. Wu, J. Xie, Z. J. Xu, S. Zhang, Q. Zhang, *J. Mater. Chem. A* **2019**, *7*, 4259–4290.
- [57] K. Wang, H. Wang, R. Bi, Y. Chu, Z. Wang, H. Wu, H. Pang, *Inorg. Chem. Front.* **2019**, *6*, 2873–2884.
- [58] C. Li, J. Xue, J. Ma, J. Li, *J. Electrochem. Soc.* **2019**, *166*, A5221–A5225.
- [59] Y. Qian, F. Zhang, H. Pang, *Adv. Funct. Mater.* **2021**, *31*, 2104231.
- [60] K. Wang, Y. Li, L.-H. Xie, X. Li, J.-R. Li, *Chem. Soc. Rev.* **2022**, *51*, 6417–6441.
- [61] J. Ren, Y. Huang, H. Zhu, B. Zhang, H. Zhu, S. Shen, G. Tan, F. Wu, H. He, S. Lan, *Carbon Energy* **2020**, *2*, 176–202.
- [62] J. Fonseca, T. Gong, L. Jiao, H.-L. Jiang, *J. Mater. Chem. A* **2021**, *9*, 10562–10611.
- [63] Y. Hu, R. Han, L. Mei, J. Liu, J. Sun, K. Yang, J. Zhao, *Mater. Today Energy* **2021**, *19*, 100608.
- [64] R. C. K. Reddy, X. Lin, A. Zeb, C.-Y. Su, *Electrochem. Energy Rev.* **2022**, *5*, 312–347.
- [65] X. Hou, C. Li, M. Li, Y. Liu, W. Zhu, Z. Li, Y. Xu, *Chin. J. Chem.* **2023**, *41*, 2597–2603.
- [66] A. Li, C. Li, P. Xiong, J. Zhang, D. Geng, Y. Xu, *Chem. Sci.* **2022**, *13*, 7575–7580.
- [67] Y. Liu, X.-Y. Xie, C. Cheng, Z.-S. Shao, H.-S. Wang, *J. Mater. Chem. C* **2019**, *7*, 10743–10763.
- [68] M. S. Yao, J. W. Xiu, Q. Q. Huang, W. H. Li, W. W. Wu, A. Q. Wu, L. A. Cao, W. H. Deng, G. E. Wang, G. Xu, *Angew. Chem.* **2019**, *131*, 15057–15061.
- [69] M. Daniel, G. Mathew, M. Anpo, B. Neppolian, *Coord. Chem. Rev.* **2022**, *468*, 214627.
- [70] G. L. Yang, X. L. Jiang, H. Xu, B. Zhao, *Small* **2021**, *17*, 2005327.
- [71] L. Wang, G.-Z. Guo, M. Wang, H.-Y. Ruan, Y.-P. Wu, X.-Q. Wu, Q.-C. Zhang, D.-S. Li, *Inorg. Chem.* **2023**, *62*, 16426–16434.
- [72] H. E. Emam, R. M. Abdelhameed, H. B. Ahmed, *J. Environ. Chem. Eng.* **2020**, *8*, 104386.
- [73] Q. Gu, H. Y. Ng, D. Zhao, J. Wang, *APL Mater.* **2020**, *8*, 040902.
- [74] M. Woellner, S. Hausdorf, N. Klein, P. Mueller, M. W. Smith, S. Kaskel, *Adv. Mater.* **2018**, *30*, 1704679.
- [75] P. M. Bhatt, V. Guillerm, S. J. Datta, A. Shkurenko, M. Eddaoudi, *Chem* **2020**, *6*, 1613–1633.
- [76] C. Gu, Z. Yu, J. Liu, D. S. Sholl, *ACS Appl. Mater. Interfaces* **2021**, *13*, 11039–11049.

- [77] F. A. Guo, J. Wang, C. Chen, X. Dong, X. Li, H. Wang, P. Guo, Y. Han, J. Li, *Angew. Chem. Int. Ed.* **2023**, *62*, e202303527.
- [78] H. Wang, S. Zhao, Y. Liu, R. Yao, X. Wang, Y. Cao, D. Ma, M. Zou, A. Cao, X. Feng, *Nat. Commun.* **2019**, *10*, 4204.
- [79] X. Ren, G. Liao, Z. Li, H. Qiao, Y. Zhang, X. Yu, B. Wang, H. Tan, L. Shi, X. Qi, *Coord. Chem. Rev.* **2021**, *435*, 213781.
- [80] M. Ding, X. Cai, H.-L. Jiang, *Chem. Sci.* **2019**, *10*, 10209–10230.
- [81] Y. Yao, C. Wang, J. Na, M. S. A. Hossain, X. Yan, H. Zhang, M. A. Amin, J. Qi, Y. Yamauchi, J. Li, *Small* **2022**, *18*, 2104387.
- [82] C. Liu, J. Wang, J. Wan, C. Yu, *Coord. Chem. Rev.* **2021**, *432*, 213743.
- [83] H. Zhou, G. Zhu, S. Dong, P. Liu, Y. Lu, Z. Zhou, S. Cao, Y. Zhang, H. Pang, *Adv. Mater.* **2023**, *35*, 2211523.
- [84] C. Liu, Y. Bai, W. Li, F. Yang, G. Zhang, H. Pang, *Angew. Chem. Int. Ed.* **2022**, *61*, e202116282.
- [85] P. Geng, L. Wang, M. Du, Y. Bai, W. Li, Y. Liu, S. Chen, P. Braunstein, Q. Xu, H. Pang, *Adv. Mater.* **2022**, *34*, 2107836.
- [86] D. Chen, W. Yang, L. Jiao, L. Li, S. H. Yu, H. L. Jiang, *Adv. Mater.* **2020**, *32*, 2000041.
- [87] H. Konnerth, B. M. Matsagar, S. S. Chen, M. H. Precht, F.-K. Shieh, K. C.-W. Wu, *Coord. Chem. Rev.* **2020**, *416*, 213319.
- [88] Z. Ye, Y. Jiang, L. Li, F. Wu, R. Chen, *Nano-Micro Lett.* **2021**, *13*, 1–37.
- [89] L. Wang, Y. Zhu, C. Du, X. Ma, C. Cao, *J. Mater. Chem. A* **2020**, *8*, 24895–24919.
- [90] J.-E. Zhou, J. Chen, Y. Peng, Y. Zheng, A. Zeb, X. Lin, *Coord. Chem. Rev.* **2022**, *472*, 214781.
- [91] Y. Shi, B. Zhu, X. Guo, W. Li, W. Ma, X. Wu, H. Pang, *Energy Storage Mater.* **2022**.
- [92] J. Cheng, Z. Liang, Y. Wu, D. Wang, T. Qiu, Y. Tang, J. Shi, D. Xia, R. Zou, *Mater. Chem. Front.* **2022**, *6*, 2184–2189.
- [93] S. Sahoo, R. Kumar, G. Dhakal, J.-J. Shim, *J. Storage Mater.* **2023**, *74*, 109427.
- [94] X. Liu, G. Verma, Z. Chen, B. Hu, Q. Huang, H. Yang, S. Ma, X. Wang, *The Innovation* **2022**, *3*, 100281.
- [95] C. Li, L. Liu, J. Kang, Y. Xiao, Y. Feng, F.-F. Cao, H. Zhang, *Energy Storage Mater.* **2020**, *31*, 115–134.
- [96] Z.-J. Zheng, H. Ye, Z.-P. Guo, *Energy Environ. Sci.* **2021**, *14*, 1835–1853.
- [97] M. Du, Q. Li, Y. Zhao, C.-S. Liu, H. Pang, *Coord. Chem. Rev.* **2020**, *416*, 213341.
- [98] M. Zhong, L. Kong, K. Zhao, Y. H. Zhang, N. Li, X. H. Bu, *Adv. Sci.* **2021**, *8*, 2001980.
- [99] L. Kong, M. Liu, H. Huang, Y. Xu, X. H. Bu, *Adv. Energy Mater.* **2022**, *12*, 2100172.
- [100] Y. An, H. Fei, Z. Zhang, L. Ci, S. Xiong, J. Feng, *Chem. Commun.* **2017**, *53*, 8360–8363.
- [101] Q. Deng, S. Feng, P. Hui, H. Chen, C. Tian, R. Yang, Y. Xu, *J. Alloys Compd.* **2020**, *830*, 154714.
- [102] Q. Deng, R. Wang, Y. Wang, Z. Yang, B. Gou, J. Li, Y. Yan, R. Yang, *J. Colloid Interface Sci.* **2022**, *628*, 556–565.
- [103] C. Li, X. Hu, B. Hu, *Electrochim. Acta* **2017**, *253*, 439–444.
- [104] X. Yin, Y. Li, W. Cai, C. Fan, W. Liu, N. Wang, G. Qin, Z. Xie, X. Chen, Y. Han, *Appl. Surf. Sci.* **2023**, *624*, 157124.
- [105] P. Mao, H. Fan, C. Liu, G. Lan, W. Huang, Z. Li, H. Mahmoud, R. Zheng, Z. Wang, H. Sun, *Sustain. Energy Fuels* **2022**, *6*, 4075–4084.
- [106] R. R. Kapaev, I. S. Zhidkov, E. Z. Kurmaev, K. J. Stevenson, P. A. Troshin, *Chem. Commun.* **2020**, *56*, 1541–1544.
- [107] C. Zhang, H. Zhao, Y. Lei, *Energy Environ. Mater.* **2020**, *3*, 105–120.
- [108] L. Deng, Z. Yang, L. Tan, L. Zeng, Y. Zhu, L. Guo, *Adv. Mater.* **2018**, *30*, 1802510.
- [109] A. Tang, X. He, H. Yin, Y. Li, Y. Zhang, S. Huang, D. G. Truhlar, *J. Phys. Chem. C* **2021**, *125*, 9679–9687.
- [110] Y. Wei, A. Tang, X. He, H. Chen, H. Yin, Y. Li, Y. Zhang, S. Huang, *J. Phys. Chem. C* **2022**, *126*, 4286–4295.
- [111] S. Li, Q. Zhang, H. Deng, S. Chen, X. Shen, Y. Yuan, Y. Cheng, J. Zhu, B. Lu, *Small Methods* **2023**, *7*, 2201554.
- [112] E. J. Canto-Aguilar, M. A. Oliver-Tolentino, G. Ramos-Sánchez, I. González, *Electrochim. Acta* **2021**, *371*, 137828.
- [113] R. R. Kapaev, A. Zhugayevych, S. V. Ryazantsev, D. A. Aksyonov, D. Novichkov, P. I. Matveev, K. J. Stevenson, *Chem. Sci.* **2022**, *13*, 8161–8170.
- [114] O. A. Kraevaya, E. V. Shchurik, P. A. Troshin, *physica status solidi (a)* **2020**, *217*, 1901050.
- [115] M. Yang, X. Zeng, M. Xie, Y. Wang, J.-M. Xiao, R.-H. Chen, Z.-J. Yi, Y.-F. Huang, D.-S. Bin, D. Li, *J. Am. Chem. Soc.* **2024**, *146*, 6753–6762.
- [116] S. Zhao, Z. Guo, K. Yan, X. Guo, S. Wan, F. He, B. Sun, G. Wang, *Small Structures* **2021**, *2*, 2000054.
- [117] J. Peng, W. Zhang, Q. Liu, J. Wang, S. Chou, H. Liu, S. Dou, *Adv. Mater.* **2022**, *34*, 2108384.
- [118] C. Zhang, K. Fan, Y. Chen, Y. Wu, C. Wang, *ACS Appl. Electron. Mater.* **2021**, *3*, 1947–1958.
- [119] W. Shu, C. Han, X. Wang, *Adv. Funct. Mater.* **2024**, *34*, 2309636.
- [120] G. He, L. F. Nazar, *ACS Energy Lett.* **2017**, *2*, 1122–1127.
- [121] W. Shu, M. Huang, L. Geng, F. Qiao, X. Wang, *Small* **2023**, *19*, 2207080.
- [122] L. Deng, J. Qu, X. Niu, J. Liu, J. Zhang, Y. Hong, M. Feng, J. Wang, M. Hu, L. Zeng, *Nat. Commun.* **2021**, *12*, 2167.
- [123] Y. Wei, S. Zhang, D. Zhai, F. Kang, *Battery Energy* **2023**, *2*, 20220027.
- [124] Y. Xia, W. Jin, Y. Qi, H. Li, Z. Jian, W. Chen, *Chin. Chem. Lett.* **2021**, *32*, 2433–2437.
- [125] C. Li, X. Wang, W. Deng, C. Liu, J. Chen, R. Li, M. Xue, *ChemElectroChem* **2018**, *5*, 3887–3892.
- [126] A. M. Rice, G. A. Leith, O. A. Ejegbawwo, E. A. Dolgopolova, N. B. Shustova, *ACS Energy Lett.* **2019**, *4*, 1938–1946.
- [127] W. Zhu, A. Li, Z. Wang, J. Yang, Y. Xu, *Small* **2021**, *17*, 2006424.
- [128] X. Bie, K. Kubota, T. Hosaka, K. Chihara, S. Komaba, *J. Mater. Chem. A* **2017**, *5*, 4325–4330.
- [129] S. Chong, Y. Wu, S. Guo, Y. Liu, G. Cao, *Energy Storage Mater.* **2019**, *22*, 120–127.
- [130] J. W. Heo, M. S. Chae, J. Hyoung, S.-T. Hong, *Inorg. Chem.* **2019**, *58*, 3065–3072.
- [131] B. Huang, Y. Liu, Z. Lu, M. Shen, J. Zhou, J. Ren, X. Li, S. Liao, *ACS Sustainable Chem. Eng.* **2019**, *7*, 16659–16667.
- [132] R. R. Kapaev, E. V. Shklyareva, G. G. Abashev, K. J. Stevenson, P. A. Troshin, *Mendeleev Commun.* **2022**, *32*, 226–227.
- [133] J. Wang, H. Jia, Z. Liu, J. Yu, L. Cheng, H. G. Wang, F. Cui, G. Zhu, *Adv. Mater.* **2024**, *36*, 2305605.
- [134] Y. Pei, C. Mu, H. Li, F. Li, J. Chen, *ChemSusChem* **2018**, *11*, 1285–1289.
- [135] Y. Sun, C. Liu, J. Xie, D. Zhuang, W. Zheng, X. Zhao, *New J. Chem.* **2019**, *43*, 11618–11625.
- [136] J. Zhang, L. Deng, M. Feng, L. Zeng, M. Hu, Y. Zhu, *Chem. Commun.* **2021**, *57*, 8632–8635.
- [137] A. Eftekhar, *J. Power Sources* **2004**, *126*, 221–228.
- [138] C. Zhang, Y. Xu, M. Zhou, L. Liang, H. Dong, M. Wu, Y. Yang, Y. Lei, *Adv. Funct. Mater.* **2017**, *27*, 1604307.
- [139] D. Su, A. McDonagh, S. Z. Qiao, G. Wang, *Adv. Mater.* **2017**, *29*, 1604007.
- [140] W. Shu, M. Huang, L. Geng, F. Qiao, X. Wang, *Small* **2023**, *19*, 2207080.
- [141] X. Wu, Z. Jian, Z. Li, X. Ji, *Electrochim. Commun.* **2017**, *77*, 54–57.
- [142] S. Chong, Y. Chen, Y. Zheng, Q. Tan, C. Shu, Y. Liu, Z. Guo, *J. Mater. Chem. A* **2017**, *5*, 22465–22471.
- [143] J. Dong, Y. Lei, D. Han, H. Wang, D. Zhai, B. Li, F. Kang, *Chem. Commun.* **2019**, *55*, 12555–12558.
- [144] X. Ma, Y. Guo, C. Yu, X. Chen, L. Gui, N. Cheng, J. Sun, P. Chen, J. Chen, Z. Zi, *J. Alloys Compd.* **2022**, *904*, 164049.
- [145] L. Xue, Y. Li, H. Gao, W. Zhou, X. Lü, W. Kaveevivitchai, A. Manthiram, J. B. Goodenough, *J. Am. Chem. Soc.* **2017**, *139*, 2164–2167.
- [146] Y. Tang, W. Li, P. Feng, M. Zhou, K. Wang, K. Jiang, *Chem. Eng. J.* **2020**, *396*, 125269.
- [147] C. D. Wessells, S. V. Peddada, R. A. Huggins, Y. Cui, *Nano Lett.* **2011**, *11*, 5421–5425.
- [148] B. Huang, Y. Shao, Y. Liu, Z. Lu, X. Lu, S. Liao, *ACS Appl. Energ. Mater.* **2019**, *2*, 6528–6535.
- [149] A. Li, L. Duan, J. Liao, J. Sun, Y. Man, X. Zhou, *ACS Appl. Energ. Mater.* **2022**, *5*, 11789–11796.

Manuscript received: March 20, 2024

Revised manuscript received: May 13, 2024

Accepted manuscript online: May 21, 2024

Version of record online: June 27, 2024